Reconnaissance geology of Lake McRae, Marlborough: Landslides, lake sediments and paleo-earthquakes

R.M. Langridge
J.M. Carey
D.T. Strong
J.D. Howarth
A. Zondervan

GNS Science Report 2015/27
February 2017

GNS SCIENCE
TE PŪ AO

DISCLAIMER

The Institute of Geological and Nuclear Sciences Limited (GNS Science) and its funders give no warranties of any kind concerning the accuracy, completeness, timeliness or fitness for purpose of the contents of this report. GNS Science accepts no responsibility for any actions taken based on, or reliance placed on the contents of this report and GNS Science and its funders exclude to the full extent permitted by law liability for any loss, damage or expense, direct or indirect, and however caused, whether through negligence or otherwise, resulting from any person's or organisation's use of, or reliance on, the contents of this report.

BIBLIOGRAPHIC REFERENCE

Langridge, R.M., Howarth, J.D., Carey, J.M., Zondervan, A., Strong, D.T. 2016. Reconnaissance geology of Lake McRae, Marlborough: Landslides, lake sediments and paleo-earthquakes, *GNS Science Report* 2015/49. 55 p.

R. M. Langridge, GNS Science, P.O. Box 30-368, Lower Hutt, New Zealand
J. D. Howarth, GNS Science, P.O. Box 30-368, Lower Hutt, New Zealand
J. M. Carey, GNS Science, P.O. Box 30-368, Lower Hutt, New Zealand
A. Zondervan, GNS Science, P.O. Box 30-368, Lower Hutt, New Zealand
D. T. Strong, GNS Science, P.O. Box 30-368, Lower Hutt, New Zealand

www.gns.cri.nz

978-0-478-19968-0 (print)
978-0-478-19969-7 (online)
ISBN 978-0-478-

CONTENTS

FIGURES

TABLES

APPENDICES

LAY ABSTRACT

Lake McRae is a small alpine (0.65 km^2, 900 m a.s.l.) landslide-dammed lake nestled within the Inland Kaikoura Ranges in Marlborough. Results from cosmogenic dating indicate that the lake formed near the end of the last ice age when two very large landslides (LS1, LS2) blocked an east-west fault-parallel valley fed mainly from Goat Valley Stream. We conducted a reconnaissance investigation of the lake and its environs, looking at the central section of the Clarence Fault adjacent to the lake, the morphology and age of the landslides, and the lake bathymetry and stratigraphy.

The Clarence Fault was mapped within the study area. The fault cuts both landslides, crosses the floor of Lake McRae and traverses a bedrock slope above the lake. A hand-dug trench into deposits at the toe of a scarp along this shutter ridge yielded colluvial deposits that are probably related to surface faulting events. Based on two radiocarbon dates, these deposits are suggestive of 1 or perhaps 2 faulting events during the last 1900-2000 years. We estimate a long term slip rate for the central section of the Clarence Fault as c. 2.8 ± 1.4 mm/yr.

Bathymetric mapping of the lake floor shows that at its western end part of landslide LS1 is submerged and draped with sediment. Shallow seismic sections indicate a layered sedimentary fill and also help to identify the Clarence Fault within the lake. Shallow (1-m) cores taken from the deepest parts of the lake penetrate the upper part of the lake section. Three radiocarbon dates help define the age structure of the uppermost lake section. Calculation of sediment accumulation rates indicates that the lake has been filled for at least 10,000 years, which is consistent with the cosmogenic ages obtained from landslide LS1.

No slump or turbidite deposits were identified in the 1-m lake cores, which suggests that there has been no shaking of Modified Mercalli (MM) intensity IX during the last 1000 years. This means that it is unlikely that the nearby Clarence or Elliott faults have ruptured during this period. Increased sediment flux into the lake has been recognised in the uppermost part of the shallow lake cores. This phenomenon is more likely related to historic farming practice (burning, clearance) and rabbit infestation during the mid-19th century, rather than being linked to a specific earthquake event such as the 1848 M 7.5 Marlborough earthquake.

Our results indicate Lake McRae formed at the end of the last ice age ($15.2^{+3.8}_{-2.7}$ thousand years ago) when two very large landslides blocked an east-west fault parallel valley. The lake has since been accumulating sediments derived mainly from Goat Valley Stream. The preliminary record from Lake McRae indicates that it has significant potential for further integrated landslide, paleoearthquake, ground motion, and lacustrine studies. In light of the recent November 14, 2016 M_w 7.8 Kaikoura earthquake sequence, further work on the active faulting and sedimentary record of this important small basin is vital.

TECHNICAL ABSTRACT

The Marlborough region is one of the most seismically and tectonically active parts of New Zealand as evidenced by the recent occurrence of the M_w 7.8 November 14, 2016 Kaikoura earthquake sequence. The Marlborough Fault System (MFS) is traversed by numerous active faults capable of producing large earthquakes Despite this little is known about its paleoseismic and geomorphic history. Lake McRae is the largest alpine lake in Marlborough and a study of its bottom sediments offered an opportunity to investigate the pre-European seismic and geomorphic history of this part of New Zealand. We undertook a reconnaissance of Lake McRae and its environs including: an investigation of the central section of the Clarence Fault; a study of the landslides that bound the lake; and, a bathymetric survey and sediment collection from the lake bed to determine its depth, age and stratigraphic characteristics.

Lake McRae is a small alpine (0.65 km^2, 900 m a.s.l.) landslide-dammed lake nestled within the Inland Kaikoura Ranges. The lake formed near the end of the last ice age when two very large landslides blocked an east-west fault-parallel valley fed mainly from the northeast by Goat Valley Stream. This project involved a reconnaissance investigation of the lake and its environs, looking at the central section of the Clarence Fault adjacent to the lake, the morphology and age of the very large landslides, and of the bathymetry, stratigraphy and chronology of deposits in the lake.

Landslide LS1 (0.5 km^2 and c. 41 x 10^6 m^3), at the western end of the lake came from the north side of the valley that parallels the Clarence Fault. Cosmogenic ^{10}Be ages of three greywacke tors and boulders protruding from the top of LS1 yield a mean age of $15{,}200^{+3800}_{-2700}$ years. Based on its morphology the larger, eastern (LS2; 0.5 km^2 and c. 70 x 10^6 m^3) landslide is probably somewhat older than LS1. LS2 was came from the southern range and collapsed to the north toward Goat Valley Stream.

The Clarence Fault was mapped within the study area. A shallow (0.7 m) trench was hand-dug into deposits at the toe of a scarp along the fault. The 2 m long trench exposed colluvial deposits derived from the slope of the shutter scarp. These deposits are mostly considered to relate to surface-faulting events that shed debris from the scarp. Based on a single radiocarbon date, these deposits indicate 1 or perhaps 2 faulting events during the last 2000 years. However, these results are unproven because fault strands were not exposed in the trench. Long-term slip rate estimates for the central section of the Clarence Fault and Elliott Fault were derived by reconstructing the history of the Acheron River, which traverses the Clarence-Elliott fault wedge from north to south. Their dextral fault slip rates are estimated at c. 2.8 ± 1.4 mm/yr and 1.4 ± 0.7 mm/yr, respectively, averaged through the Quaternary period.

The lake has a maximum water depth of c. 43 m. The bathymetry indicates the hummocky morphology of part of landslide LS1 on the floor of the lake at its western end. Sub-bottom CHIRP (shallow geophysical) sections indicate a layered sedimentary lake fill with an estimated thickness of up to 10 m. The CHIRP sections also help to identify the Clarence Fault in the subsurface in the southwest corner of the lake. Shallow (1-m) cores were taken from the deepest parts of the lake and penetrate the upper part of the lake section. The lake fill is comprised of fine-grained layered sedimentary packages. A basal radiocarbon date on plant fragments from these cores (at a depth of 0.64 m) is 416 ± 22 yr B.P. Projection of the rates of recent sediment accumulation implies that the lake has been filled (and accumulating layered lake sediments) for at least 10,000 years. This age is consistent with the cosmogenic 10Be ages from landslide LS1.

No lacustrine mass-wasting deposits were identified in the 1-m cores, which suggests that there has been no shaking of Modified Mercalli (MM) intensity IX during the last 1000 years. This means that it is unlikely that the Clarence or Elliott faults have ruptured during this time period. Increased sediment flux into the lake has been recognised in the uppermost part of the shallow lake cores. This phenomenon is believed to be related to recent strong shaking (MMI ≥VIII) from a regional fault source. Seismic shaking from the historical rupture of the eastern Awatere Fault during the M 7.5 1848 Marlborough earthquake is considered to be the best candidate for such a change in the sediment flux coming from Goat Valley Stream. Other regional historical shaking events such as the 1855 Wairarapa, 1888 Amuri and 1929 Buller earthquakes may have been distant or weak enough to have not generated increased sediment flux or failure within the lake.

Our reconnaissance study of Lake McRae indicates that it has significant potential for further landslide, paleoearthquake, ground motion, and lacustrine studies and also has potential as a site for paleoclimate study. Future research at the lake could include intermediate (6-m) depth coring of sediments, further cosmogenic dating of the landslides and study of the activity and paleoseismicity of the Clarence Fault. In light of the recent November 14, 2016 M_w 7.8 Kaikoura earthquake sequence, further work on the active faulting and sedimentary record of this important small basin is vital. The effects of shaking and turbidity related to the Kaikoura earthquake should be a tractable target of future research.

KEYWORDS

Lake McRae, landslide-dammed lake, paleoseismicity, Clarence Fault, turbidite, Cosmogenic dating, LiDAR

1.0 INTRODUCTION

1.1 BACKGROUND

Recent moderate to large earthquake sequences in New Zealand, e.g. Fiordland 2003-2009, Canterbury 2010-2016, 2013 Cook Strait and the 2016 Kaikoura earthquake have highlighted the occurrence of earthquake-induced landslides, and building and infrastructure damage and loss of life (e.g. Reyners et al., 2003; Kaiser et al., 2011; Khajavi et al., 2012; Hamling et al., 2014; Hancox et al., 2014). Landscape features in a tectonically active country like New Zealand also offer the opportunity to test the recurrence of shaking of stable and unstable landforms (Stirling and Anooshehpoor, 2006). Recent studies into the timing of very large to giant mass movement features have categorised many as earthquake-induced landslides (EILs), dating from the early Holocene when steep alpine valley sides were released from glacial ice (Hancox and Perrin, 2009; Hancox et al., 2013). These features together with a broader catalogue of historical earthquakes and associated EILs in New Zealand (Adams, 1981; Hancox et al., 2002) indicate that the typical ground shaking intensities required to cause bedrock hillslope failures (landslides) are of Modified Mercalli Intensity (MMI) VIII or greater.

Determining relationships between large EILs and their shaking sources (an active fault) allows regional assessments of the impacts of historical earthquakes in New Zealand e.g. 1929 M_w 7.1 Arthurs Pass, 1929 M_w 7.8 Murchison and 2016 Kaikoura earthquakes (Hamling et al., in review; Hancox et al., 2002) as well as globally e.g., 2005 M_w 7.6 Kashmir, 2008 M_w 7.9 Wenchuan, 2015 M_w 7.8 Gorkha earthquakes along the mountainous belts of southern Asia. Whilst such records provide essential data to evaluate the impacts of active faults, longer records of ground shaking are needed to fully inform assessment of potential impacts and future risks.

Recent research, has demonstrated that lakes can be sensitive recorders of past shaking. For example, West Coast lakes have provided high quality records of proximal to distal shaking events produced by the Alpine Fault (Howarth et al. 2012; 2013). It has been deduced that shaking intensities of MM VII or greater can generate subaqueous failure of lake sediments that are redeposited as mass wasting deposits and/or as turbidites in the depocentres of lakes. These findings provide new methods to assess ground shaking events using lakes in other areas of New Zealand (Howarth et al., 2012, 2014, 2016), and here we apply it for the first time in the Marlborough Fault System.

Lake McRae is a small, alpine landslide-dammed lake (LDL) in the eastern part of the Marlborough Fault System (MFS; Figure 1.1). The lake results from two very large landslide deposits that dammed the valley along the trend of the Clarence Fault in the Inland Kaikoura Ranges. It has been previously suggested that Lake McRae formed some time since the last glacial period (Alloway et al., 2007; Barrell et al., 2011) but little is known about the time of its formation and what triggered the landslides.

Lake McRae hosts sediments with potential to yield a record of strong shaking caused by large earthquakes. In this project we test whether the lake may be a “paleo-seismometer”, that is, a natural recorder of shaking from local, regional and possibly distal earthquake fault sources.

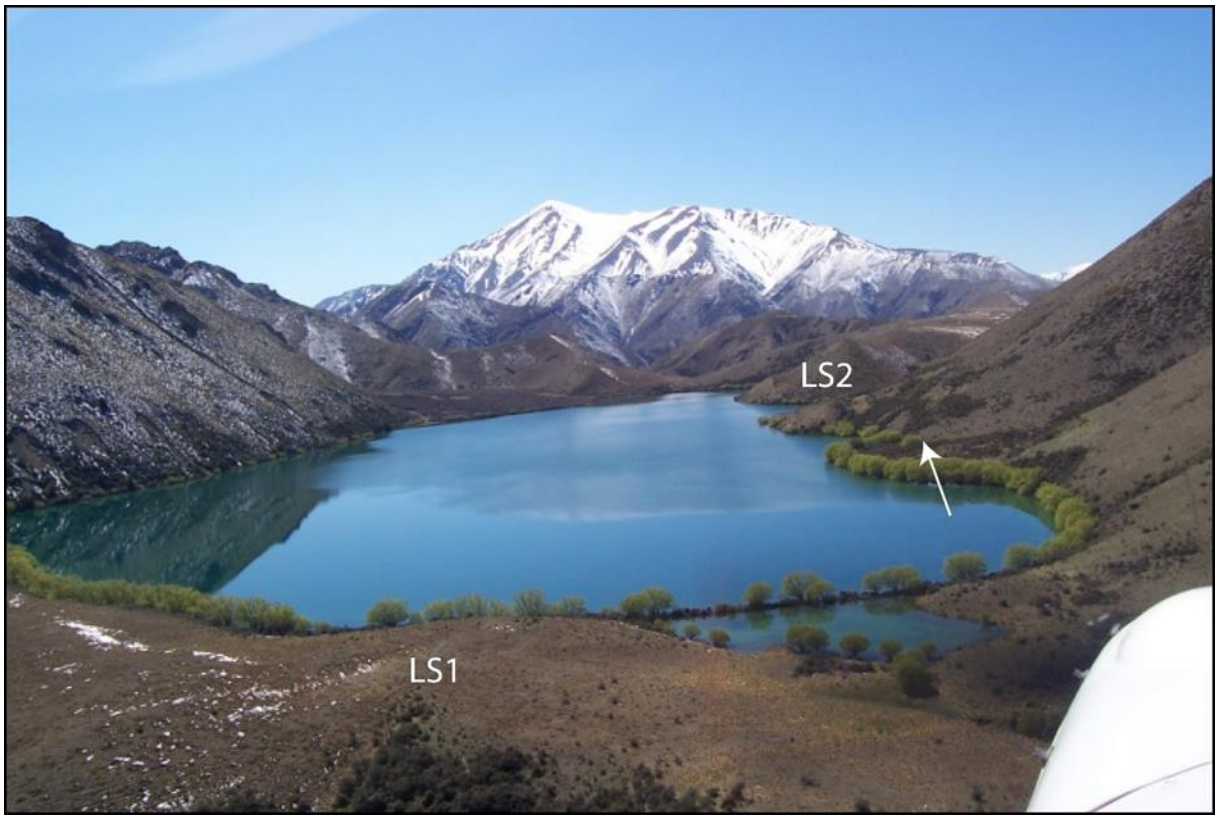

Figure 1.1 Lake McRae viewed from the west. The lake is c. 1.5 km long and 0.5 km wide. One of two large landslide deposits (LS1) occurs in the foreground, while the other (LS2) occurs at right, in the middle distance. The Clarence Fault occurs along the rangefront on the south side of the lake (white arrow). Mt. St. Bernard (2256 m a.s.l.) is the highest peak in the background.

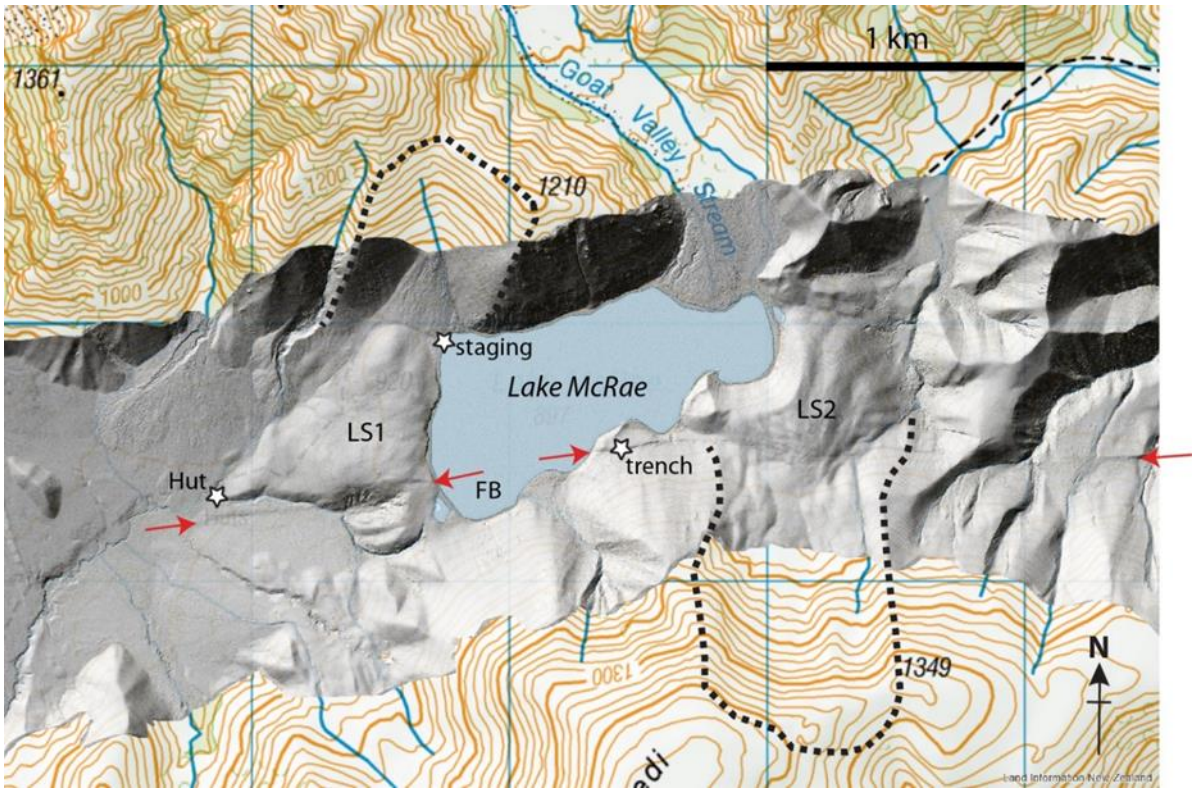

Figure 1.2 Lake McRae and environs. The source areas (head- and side-scarps) of landslide deposits LS1 and LS2 are marked by dashed black lines. The active trace of the Clarence Fault is marked by red arrows. Goat Valley Stream is the major catchment entering Lake McRae. Important sites are marked by stars. Boat access to the lake was staged from the northwest corner of the lake. FB = Fault Bay.

In this study we attempted to determine the ages of the landslides that led to the formation Lake McRae. We also investigated the sediment deposited in the lake using geophysical surveys and cores from the lake bottom to determine the age of the lake and its rate of sedimentation since it formed. We combined these with the history of recent fault movements along the adjacent Clarence Fault to develop an alpine shaking/landsliding/fault rupture and lake sedimentation framework. Within eastern Marlborough, Lake McRae is unique in providing the opportunity for such an integrated hazard study. Our results provide new insights into the causes, return periods and timings of strong shaking (MMI ≥VIII) in an important New Zealand alpine setting. Such data may be used for assessing and validating regional shaking models supplied by the National Seismic Hazard Model (NSHM; Stirling et al., 2002, 2012).

1.2 PROJECT SCOPE

The aims of the study were to investigate the timing of the landslides that dam Lake McRae in the Inland Kaikoura Ranges (Figure 1.1), the record of lake sediments filling the subsequent lake, and the history of recent fault movements along the adjacent Clarence Fault in an integrated fashion that links together these hazards.

In March 2015, we undertook a field reconnaissance to:

1. Map the Lake McRae landslides and locate exposures into them
2. Survey the bathymetry and structure of the lake bottom sediments
3. Obtain sediment cores that could potentially contain deformed and dateable packages of lake sediments
4. Map offsets and locate exposures along the active trace of the Clarence Fault
5. Collect organic material for radiocarbon dating and/or sediment samples for OSL dating in order to constrain the age of the landslides, Lake McRae and its sediments, and of the timing of paleo-shaking/rupture events from these records.

The project was aided by the acquisition of airborne LiDAR along the central part of the Clarence Fault, which includes coverage of Lake McRae (Figure 1.2). In addition, a GNS Direct Core Funding grant from the Landslide Hazard Platform was used to obtain Cosmogenic ages for the landslides using rocks exposed in the landslide debris.

A summary of the field reconnaissance is described in Appendix 1. In addition to this report, we aim to write a scientific paper that focuses on the most relevant results of this study.

1.3 REPORT STRUCTURE

The report is divided into the following chapters:

- Chapter 2 provides the study Background, including the regional tectonics and geology relating to the Lake McRae area;
- Chapter 3 present findings from the Clarence Fault investigations, including active fault reconnaissance mapping, displacement, slip rate and on-fault paleoseismic data
- Chapter 4 presents findings from the Landslide Investigations, including reconnaissance, sample site selection, and cosmogenic dating
- Chapter 5 presents findings from the Lake Investigations, including lake survey and bathymetry, coring of lake sediments and age models

- Chapter 6 provides a Discussion including the interpretation and integration of the three main datasets
- Chapter 7 provides the Conclusions of the study.

2.0 BACKGROUND

2.1 INTRODUCTION

The Marlborough region spans an on-land distributed plate boundary zone, known as the Marlborough Fault System (MFS), across which transpressional deformation between the Australian and Pacific plates is accommodated (DeMets et al., 1994; Wallace et al., 2007). Much of this deformation is distributed across several upper plate strike-slip faults; chiefly the Hope, Clarence, Awatere and Alpine-Wairau faults (Van Dissen and Yeats, 1991) (Figure 2.1).

Lake McRae, set in the Inland Kaikoura Ranges at 900 m a.s.l., is one of the largest lakes (c. 0.65 km^2) within the Marlborough region. It is a landslide-dammed lake (LDL); large landslides exist at the western and eastern ends of the local valley (Figure 1.2; Figure 2.3). Previous studies indicate that the Clarence Fault disrupts both landslide deposits and part of the lake floor (Figure 1.2) (Kieckhefer, 1979; Rattenbury et al., 2006). The lake is predominantly fed by Goat Valley Stream, which drains into the lake from the north. A preliminary estimate of the valley profile from a 15-m DEM indicate that the lake could be tens of metres deep.

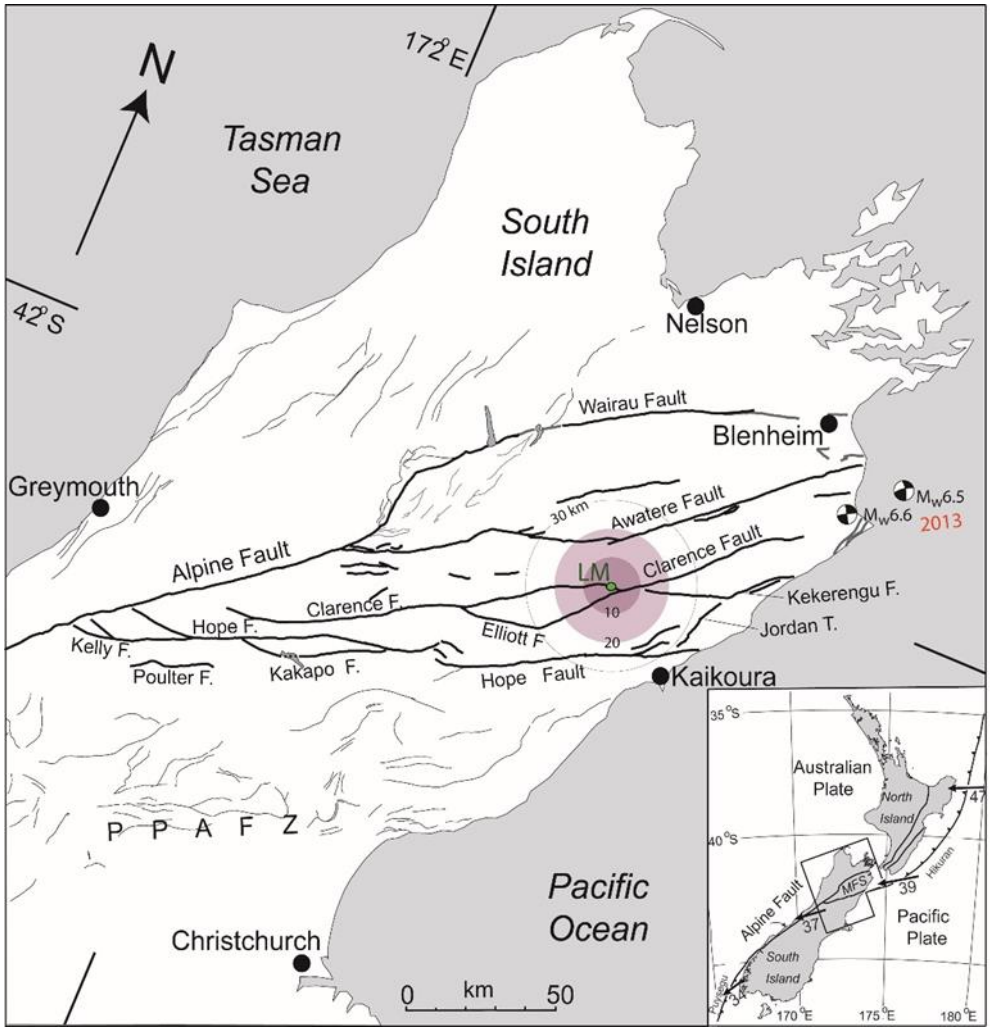

Figure 2.1 Active fault map of the Marlborough Fault System (MFS) in the northern South Island. Contour lines around the lake indicate the distance from the lake to seismic sources; contours could roughly be inverted to shaking intensity from a point source. Beach balls highlight the main shocks from the 2013 Cook Strait seismic sequence. Inset: the tectonic setting of New Zealand and rates of tectonic motion across the Australia-Pacific plate boundary.

Lake McRae provides an opportunity to improve knowledge on the damaging impacts of future earthquakes in alpine environments. Importantly, there are few extended paleo-earthquake

histories for the major faults in the Marlborough Fault System. Figure 2.1 shows how Lake McRae could be uniquely situated to record earthquake shaking and ground motions from historical and large paleo-earthquakes. The lake is situated along the central segment of the Clarence Fault, 3 km from the Elliott Fault and 5 km from the eastern segment of the Clarence, 18 km from the Awatere and 25 km from the Hope faults. As a consequence, the lake sediments may have recorded a range of MM intensities since its formation. If the lake is old enough, then its sediments are likely to have recorded MM intensities of ≥VII and therefore are likely to yield a record of turbidites or soft-sediment deformation (e.g. Howarth et al., 2012). Insights from other alpine areas in the South Island suggest that the landslide deposits damming the lake are likely to be of early Holocene age, post-dating the last glacial period (Adams, 1981; Hancox et al., 2013). Strong shaking at the lake, from the fault sources listed above, will likely range from MMI VII to MMI IX. As such, the lake may provide one of the best tests of the time-averaged ground motions modelled in the NSHM (Stirling et al., 2012). As there are no similar lakes within 40 km of this site, it probably also represents the best opportunity to view a long record of earthquake shaking in eastern Marlborough (Figure 2.1).

Recent studies and historical earthquakes indicate that strong ground motions from large to great seismic sources can destabilise the terrain in mountainous areas, causing earthquake-induced landslides (EILs). In the South Island, the Southern Alps are rich in earthquake source faults and landslide deposits are evident throughout the landscape. Many of these have been linked to historical seismicity, e.g. Falling Mountain landslide derived from the 1929 Arthurs Pass earthquake (Speight, 1933; Hancox et al., 2002), or to paleoseismic events such as the Round Top landslide along the Alpine Fault (Wright, 1998).

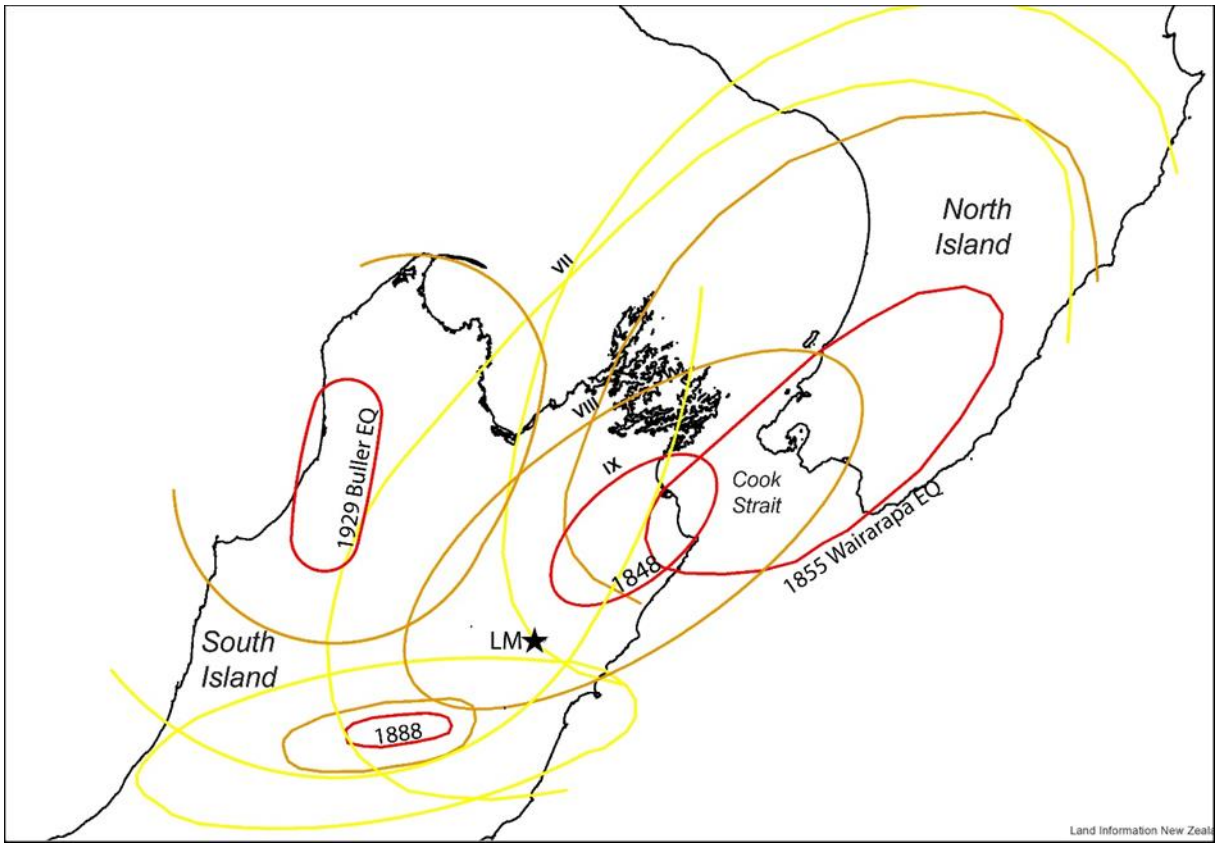

Figure 2.2 MM Intensity contours (VII-IX) for the 1848 Marlborough, 1855 Wairarapa, 1888 Amuri and 1929 Buller earthquakes (source: Downes and Dowrick, 2014). Lake McRae (LM) is identified by a star.

We should expect to observe deformation and/or increased sediment flux in the lake sediment record of Lake McRae in response to medial historical earthquakes or indeed paleoseismic

events on nearby faults, especially the Clarence Fault. Figure 2.2 shows isoseismal Modified Mercalli (MM) Intensity contours for four of the largest historical earthquakes in central New Zealand (Downes and Dowrick, 2014). These events are the: 1848 M 7.4-7.5 Marlborough, 1855 M_w 8.2 Wairarapa, 1888 M_w 7.1 North Canterbury (Amuri), and 1929 M_w 7.8 Buller earthquakes (Cowan, 1991; Downes and Dowrick, 2014; Grapes et al., 1998; Stirling et al., 2012; Khajavi et al., 2016).

In particular, Figure 2.2 displays the higher isoseismals of MM VII to IX as these fields highlight where strong to intense shaking is likely to have occurred during those earthquakes. Thus, Lake McRae can be treated as a location that has its own site effects with respect to individual earthquakes. The lake occurs within the MM VII isoseismal for two of the four earthquakes (1855 and 1929) but occurs slightly beyond the MM VII isoseismal for the 1888 Amuri earthquake. For the 1848 Marlborough earthquake, the lake occurs within the MM VIII intensity contour. MM Intensity VII is accepted as the minimum intensity required to generate significant catchment-wide landsliding as a result of strong shaking. Similarly, it is also the minimum threshold at which mass wasting has been assigned to deformation and/or catchment perturbation within the sedimentary records of West Coast lakes (Howarth et al., 2012; 2014; 2016).

Based on data from GeoNet, during the 14 November, 2016 M_w 7.8 Kaikoura earthquake, the location of Lake McRae should have been subjected to vertical accelerations of 0.2-0.3 g, horizontal accelerations of 0.3-0.45, and an MM Intensity of V-VI (www.geonet.org.nz). No felt reports were submitted from anywhere within 40 km of Lake McRae.

Figure 2.3 Lake McRae viewed from the east. The fan-delta of Goat Valley Stream appears at lower right. The subaerial part of landslide deposit LS1 forms the straight, western shore of the lake in the distance.

Figure 2.4 Oblique aerial view of the southern side of Lake McRae. The vegetation lineament running along the base of the range highlights the trace of the active Clarence Fault (red arrows). Photo: Matt Hill.

We hypothesised that Lake McRae formed during the early Holocene via landslide blockage, and has since been infilling with sediments from the Goat Valley Stream catchment, the erosion of the two large landslide deposits and erosion from the surrounding slopes (Figure 2.3). These sediments have in turn been subjected to faulting and shaking from movements on the Clarence Fault, and shaking by large to great (M_w ≥7) regional earthquakes on other faults, especially those passing within 30 km of the site (Figure 2.1). The Lake McRae landslide deposits are likely to be EILs (Adams, 1981) that have subsequently been displaced by the Clarence Fault, implying that the lake pre-dates the most recent large earthquake (or earthquakes) on the Clarence Fault there (Figure 2.4).

2.2 GEOLOGY, VEGETATION AND CLIMATE

The average annual rainfall in this area is c. 1200-1600 mm/yr (NIWA rainfall statistics). The local vegetation currently is dominated by grassland with sweet briar and Matagouri at lower elevations and short tussock to snow tussock grassland at higher elevations (Newsome 1987). Willow trees are common around the shores of Lake McRae and pockets of beech forest exist locally in sheltered south-facing side valleys (Figure 2.3).

Geologically, Lake McRae occurs in a mountainous landscape where the geology is dominated by ranges comprised of Cretaceous (Torlesse Pahau) greywacke rocks (Rattenbury et al., 2006) (Figure 2.5). While no Tertiary rocks have been mapped near the lake, these rocks likely

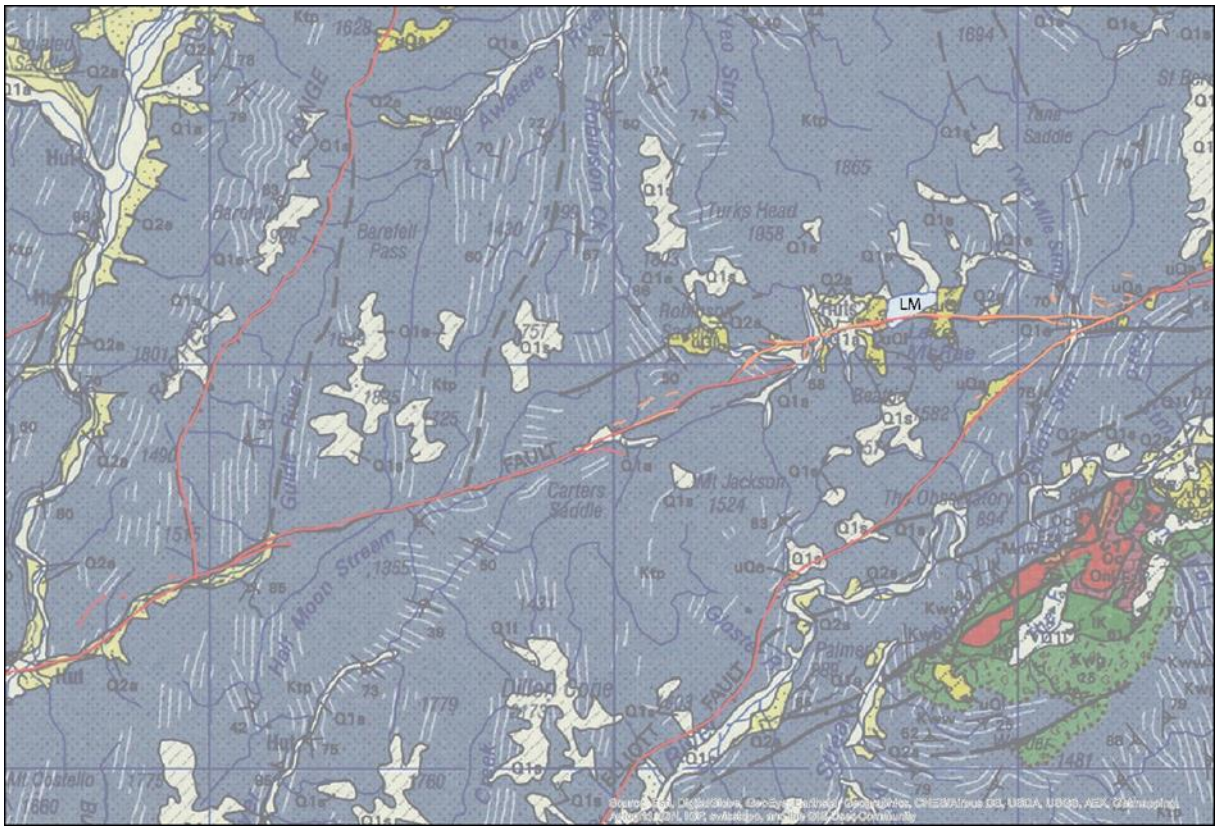

Figure 2.5 Bedrock geology of the Lake McRae area extracted from Rattenbury et al. (2006). The lake (LM) is at centre right. Active faults are shown with red lines. Cretaceous Pahau greywacke is shown in purple. Tertiary rocks are shown in green and orange. Quaternary deposits are shown in yellow and beige.

existed across the region prior to the ongoing deformation (uplift) and erosion associated with faults of the MFS throughout the late Tertiary (Van Dissen & Yeats, 1991; Little and Jones, 1998). Remnants of Tertiary basins exist to the southeast of the Elliott Fault (Figure 2.5). Rattenbury et al. (2006) indicate the presence of Quaternary deposits in the area near Lake McRae. These include alluvium (Q2a, Q1a), landslide deposits (uQl) and scree deposits (Q1s).

The Clarence and Elliott faults are major active faults that traverse this part of the MFS. The eastern segment of the Clarence Fault bifurcates c. 5 km east of Lake McRae, becoming the Elliott Fault and the central section of the Clarence Fault (Figure 2.5).

3.0 CLARENCE FAULT INVESTIGATIONS

The northeast-striking Clarence Fault is recognised as one of the four main strike-slip faults of the Marlborough Fault System (Van Dissen, 1989; Van Dissen & Yeats, 1991). The Clarence Fault can be divided into three sections: the eastern, central and western sections. Much of the neotectonic research undertaken along the fault has been focused in the eastern part of the Clarence Fault which is more easily accessed (Browne, 1992; Nicol and Van Dissen, 2002; Townsend and Little, 1998; Van Dissen and Nicol, 2009). The central section of the Clarence Fault is coincident with the part of the fault where it is divided into the Clarence and Elliott faults (Eusden et al., 2012). In the east, the Clarence and Elliott faults bifurcate near Elliott Stream, while in the west, they separate near the Rainbow Road and the Clarence Fault continues as a single structure toward the Alpine Fault (Langridge 2004). The area across which the Clarence Fault is linked with the Elliott Fault has been called the Clarence-Elliott fault wedge (Kieckhefer, 1979; Eusden et al., 2012).

The first detailed mapping along much of the central Clarence Fault, including in the vicinity of Lake McRae, was undertaken by Kieckhefer (1979). Kieckhefer mapped discontinuous traces of the fault within the study area adjacent to the Lake McRae. He also notes several observations of scarps, springs and vertical and horizontal displacements within 2 km of the lake. Along the eastern section of the Clarence Fault, the structural analysis of oblique-slip faulting has resulted in a Holocene dextral slip rate determination of 3.5-5 mm/yr (Nicol and Van Dissen, 2002). Van Dissen and Nicol (2009) suggest a dextral slip rate of c. 4 mm/yr. In addition, paleoseismic data indicate four mid to late Holocene earthquake rupture events on the eastern segment of the Clarence Fault, yielding a recurrence interval of c. 1700 years (Van Dissen and Nicol 2009). The timing of the most recent earthquake occurred 1700-1900 calibrated years before present (BP).

3.1 CLARENCE FAULT MAPPING

Reconnaissance of the lake and its geomorphic environs was initially undertaken to map the Clarence Fault and to locate possible sites where datable material could be used to constrain slip rate, slip or paleo-earthquake ages. We undertook a reconnaissance along the main trace of the Clarence Fault. Field reconnaissance was supported by additional mapping of the Clarence Fault on LiDAR images and within the lake in 'Fault Bay' (Figure 2.4).

At the western shore of Lake McRae, there is no clear evidence that the shoreline or beach ridges are displaced by the fault. The expression of the fault within Fault Bay is discussed in Chapter 5. East of Fault Bay, the fault is expressed by a south- and uphill-facing scarp (shutter ridge) of up to 5 m height (Kieckhefer 1979; this study). This part of the fault is expressed as a sharp, linear scarp trending at 080-085°, that both ponds and deflects drainage, resulting in boggy ground along the fault trace (Figure 2.4). Greywacke exposed in cliffs along the lake and in the rangefront indicates that bedrock cores the shutter ridge on both sides of the fault.

West of Fault Bay the Clarence Fault is marked by an active trace that displaces landslide LS1 associated with a south-facing fault scarp. A line of springs and a vegetation anomaly is associated with this trace (Figure 3.2). Near Lake McRae Hut it is likely that springs and clusters of trees are associated with upflow of water along the fault. In this area, Kieckhefer (1979) notes an up-to-the-north scarp of 30 cm height striking at 079º. We note from the LiDAR that c. 1 km west of Lake McRae Hut alluvial surfaces of presumed Holocene age are faulted, with vertical and dextral displacements.

At the south-eastern end of the lake, the surface trace of the Clarence Fault cuts across landslide deposit LS2 (Figure 3.3). The trace cuts the landslide in its upper reaches between the source area and the head of the deposit, where there is relatively level ground. Small drainages emanating off the landslide scar appear to be deflected to the right across the rumpled ground corresponding to the fault zone. A traverse of landslide LS2 marked the eastern limit of our reconnaissance mapping of the fault and landslides.

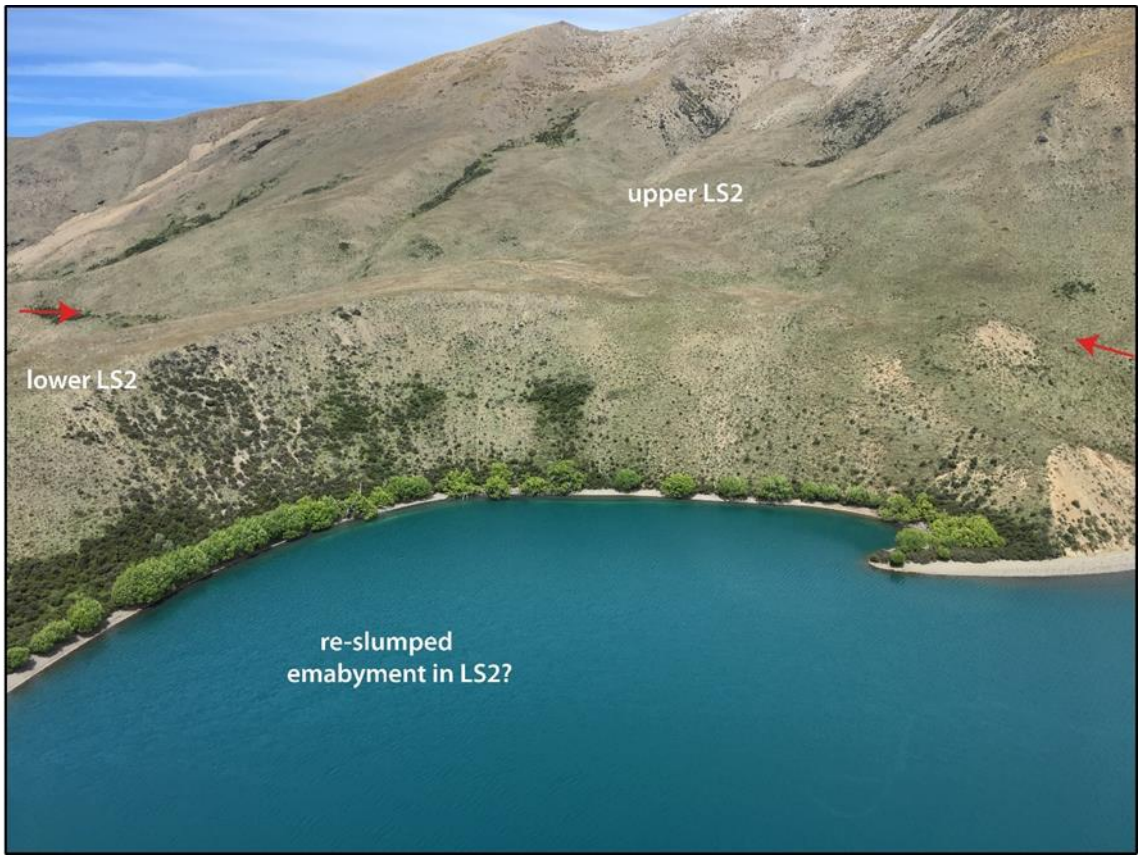

Figure 3.1 Aerial view of LS2 landslide deposit from the north. The upper part of LS2 below the source area is characterised by hummocky ground. The Clarence Fault cuts across LS2 in the mid-ground. The lower part of LS2 is a large mass failure that has arguably re-slumped to form a large embayment in the lake. Photo: Matt Hill.

In summary, the location of the active, dextral-slip Clarence Fault was confirmed across the study area. The fault is expressed most clearly by vertical scarps, with few new observations of dextrally-offset markers. The fault was observed across both LS1 and LS2 landslides which indicates that the landslides pre-date at least the most recent movement on the Clarence Fault. The shutter ridge east of Fault Bay was probably formed by multiple fault movements. Offset terraces west of Lake McRae Hut indicate that the fault was probably active during the mid to late Holocene. The size of fault scarps (i.e. the amount of expression of deformation) across the LS1 deposit suggests that the landslide deposit is relatively old or has been deformed by multiple fault displacements.

3.2 CENTRAL CLARENCE FAULT SLIP RATE

To assess the slip rate of the central section of the Clarence Fault, we considered a novel geologic approach to apportioning slip rate between the Clarence and Elliott faults. This approach uses reconstructions of the Acheron and Clarence rivers that cross both the Clarence and Elliott faults (Figure 3.4). The assumptions behind this reconstruction are that:

- The current rate of 3.5-5 mm/yr on the eastern Clarence Fault is apportioned sub-equally to the two faults
- The bends in the Acheron and Clarence rivers are caused by long-term right-lateral displacement of their river valley axes
- The Clarence and Acheron rivers were both formerly south-flowing rivers, and that the Acheron River was captured by the Clarence River northeast of Hanmer Springs.

Taking these assumptions into account, it is possible to produce reconstructions of c. 5.0 ± 0.2 km of dextral slip on the central section of the Clarence Fault, as evidenced across the Acheron River, and c. 2.5 ± 0.2 km of dextral slip on the Elliott Fault, as evidenced across the southernmost portion of the Acheron River (now captured by the Clarence River). The uncertainties on these values are minimums, however, the values themselves provide a ratio of displacement partitioning between the two faults of c. 2:1. In concert with the contemporary slip rate from the eastern Clarence Fault (4.25 ± 0.75 mm/yr) it is possible to estimate slip rates of c. 2.8 and 1.4 mm/yr for the central Clarence and Elliott faults, respectively.

In terms of earthquake displacement and recurrence interval these values imply that the faults accumulate c. 2.8 and 1.4 m of slip every 1000 years, respectively. In terms of long-term displacement, assuming constant slip rate over time, these rates also indicate long term displacements of c. 2.8 and 1.4 km per million years. If the two faults have accumulated their own displacements at their current rates, then it could be inferred that the offsets of these river valleys has accrued over the last c. 1.8 Ma or so. Given the uncertainties on displacement and assumptions this age broadly coincides with the onset of the Quaternary period. We argue here that when glaciations became more pronounced in the early Quaternary, that rivers like the Acheron probably became more entrenched. Thus the current valley forms of the Acheron and Clarence rivers could have found their courses during the early Quaternary when fluvial and glacial processes were enhanced. We assert that at this time the Clarence and Acheron rivers were flowing to the south away from the Alpine (Southern Alps) orogeny. This was possible prior to the inception of the Hope Fault and the uplift of the Hanmer Range in response to the formation of the Hanmer Basin. Langridge et al. (2013) suggest that displacement across bedrock markers has been accruing on the western part of the Hope Fault since 0.6-1.6 Ma.

We suggest an uncertainty on the Clarence and Elliott fault slip rates of ±50% to reasonably account for uncertainties in rates on the million-year time scale. Thus the rates we suggest for the central Clarence Fault and Elliott Fault are 2.8 ± 1.4 mm/yr and 1.4 ± 0.7 mm/yr. If these uncertainties are propagated into the time accrued for long-term displacements, then the period over which the associated displacements could accrue is c. 1.5-2.15 Ma, which spans the early Quaternary period.

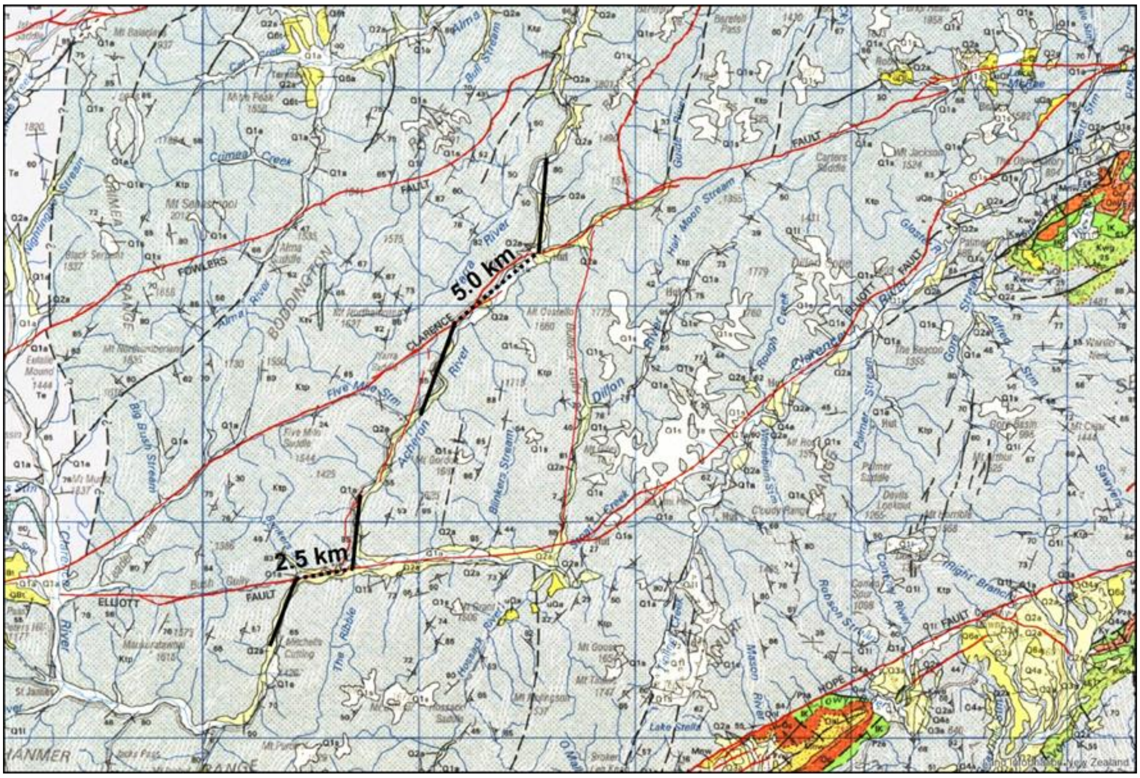

Figure 3.2 Geology of the Clarence-Elliott fault wedge within the central Marlborough Fault System highlighting possible offset river courses across the two faults (geology from Rattenbury et al., 2006). The northern displacement of 5 km is measured across the Acheron valley on the Clarence Fault. The southern displacement of 2.5 km is measured across the Acheron-Clarence valleys on the Elliott Fault.

CLARENCE FAULT EXCAVATION

To investigate the record of recent paleoseismic events a shallow hand-dug trench (2-m long and 0.75 m deep) was excavated at the foot of the shutter scarp along the Clarence Fault south of Lake McRae (Figure 1.2, Figure 3.3). The trench exposed a sequence of unfaulted deposits from which charcoal and sediment samples were collected for radiocarbon, and infra-red stimulated luminescence (IRSL) dating, respectively (Figure 3.3, Figure 3.4).

3.3.1 Stratigraphy and Chronology of Deposits

Figure 3.5 shows the log of the Lake McRae trench. The stratigraphy is comprised of a sequence of unfaulted, trough-filling deposits of colluvium and alluvium capped by a recent soil, as follows:

- The uppermost unit at the ground surface is a silt loam (soil, unit 1a) formed into a thin silt deposit (unit 1) and into slope deposits (unit 1c) at the toe of the shutter scarp. Several small pieces of charcoal were recovered from the Unit 1 silt. The charcoal was dated at the Rafter Radiocarbon Lab and yielded an age of 144 ± 19 yr BP (0-258 cal yr BP). A sediment tube was also taken from unit 1 for IRSL dating. This date probably reflects European burning. A preliminary Infra-red Stimulated Luminescence (IRSL) lab date on quartz grains from this silt yielded an age of 0.29 ± 0.03 ka, which is consistent with the radiocarbon age.
- Unit 2C is a fine angular greywacke grit that thins off the scarp beneath unit 1. Unit 2C has a matrix of medium silt with brown soil colours. We interpret 2C as a colluvium derived from the scarp comprised of a mix of reworked soil and greywacke clasts. The origin of 2C and the overlying silt are discussed further below.

- Unit 3a is a weak paleosol formed into unit 3C. The thin paleosol is characterised by light brown grey silty sandy gravel. Unit 3C fines upward and to the south, and has an average clast size of 2 cm. Unit 3C is a light brown-grey silty, sandy gravel. Sediment tubes were collected from unit 3C and from the underlying unit (4C). Unit 3C is interpreted as a scarp-derived colluvium.
- Unit 4C is a white gravelly silt with a firm nutty texture and a bleached white silty matrix with a vesicular texture. We interpret this unit as either basal facies related to unit 3C, or a bleached and buried soil formed into colluvium that drapes over unit 4X. The latter is our preferred option, especially if the vesicular and bleached nature of unit 4C is related to shallow soil processes. A single piece of charcoal collected from unit 4C yielded a radiocarbon age of 2034 ± 20 yr BP (1900-2003 cal yr BP).
- Unit 4X occurs in the southern end of the trench only near the floor. This deposit comprises angular clasts of unweathered greywacke. Its exposure suggests that it thickens and coarsens to the south. As such, it is suggested that unit 4X is derived from the southern bedrock hillslope rather than the shutter scarp. In general, the clasts in unit 4X are much larger (average 10 cm, largest clast 26 cm) and more competent than those from the other units in the trench (i.e. 2C, 3C, 4C), that are typically nutty (equant) fine gravels. These properties indicate that unit 4X could be a scree deposit from the rangefront rather than the shutter scarp.

Figure 3.3 Location of the trench dug across the trace of the Clarence Fault into the toe of a shutter scarp. Location of the trench dug across the trace of the Clarence Fault into the toe of a shutter scarp. The uphill-facing scarp at this location is c. 4 m high here.

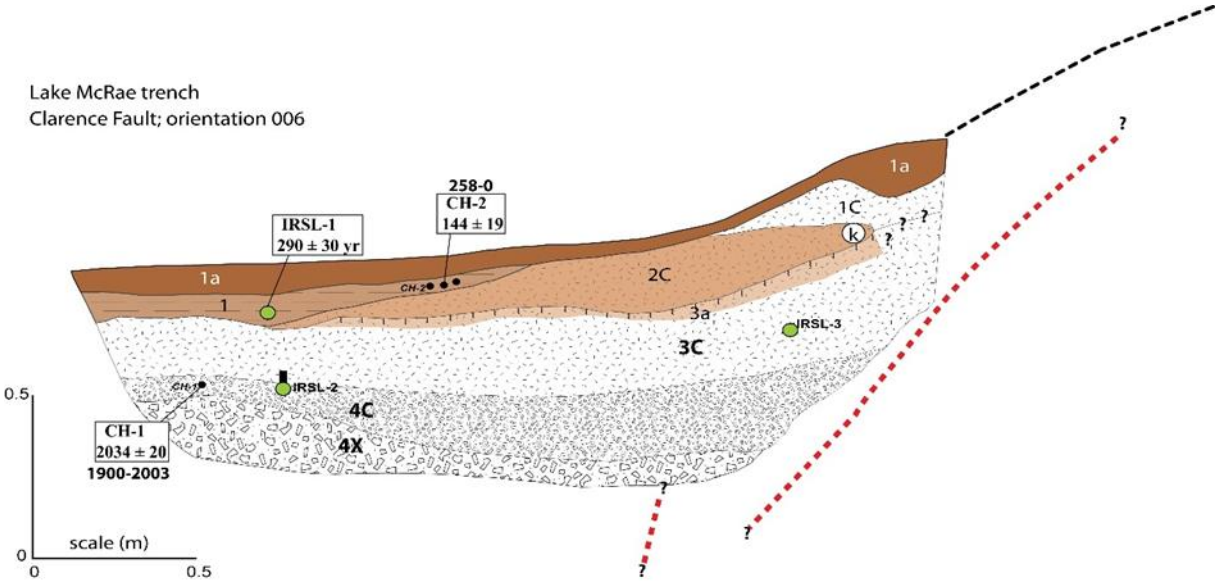

Figure 3.4 Log of the Lake McRae paleoseismic trench hand-dug along the active trace of the Clarence Fault. The deposits shown are indicative of scarp-derived colluviums and soils. However, no faults were exposed in the trench, hence only possible fault locations and dips are suggested. Unit 3a marked with ticks is a buried soil (paleosol). Radiocarbon ages in bold are in calibrated yr BP. Green circles show IRSL sediment tube samples.

Table 3.1 Radiocarbon dates from the Clarence Fault (Lake McRae) trench.

Sample ID	Description	Fraction dated	NZA	CRA [yBP]	CRA error	$\delta^{13}C$ [‰]	$\delta^{13}C$ error
CH-2	charcoal	charcoal grains	59057	144	19	-24.3	0.2
CH-1	charcoal	charcoal grain	59056	2034	20	-23.6	0.2

3.3.2 Interpretation

The trench did not expose any faults, therefore it is difficult to interpret the record of faulting and the timing of displacements on the Clarence Fault. However, the stratigraphy and dates provide some insight into the rejuvenation of the scarp, which is arguably related to surface faulting.

Colluvial unit 2C buries a paleosol on unit 3a and so may be a scarp-derived colluvium, i.e. a colluvium generated through faulting. However, we err on the side of caution for explaining the origin of this unit because it is young and bioturbated. It is possible that the surficial units (units 1, 1a, 1C and 2C) all formed following the beginning of farming on Molesworth Station, and in particular could have been derived from erosion due to an explosion of rabbits in Marlborough. To support this, we note that a rabbit burrow was logged in the trench (k = krotovina) within unit 2C. These surficial units may all be relatively young as suggested by the radiocarbon (CH-2; 144 ± 19 yr) and the IRSL date from the unit 1 silt (290 ± 30 yr). There is no known historical rupture of the Clarence Fault to account for a very young surface faulting event. Based on this we consider that the colluvium beneath paleosol 3a (i.e. unit 3C) is the most likely candidate to be related to the most recent faulting event. The timing of this event must post-date radiocarbon date CH-1 (2034 ± 20 yr; 1900-2003 cal yr BP) or be equivalent to it. IRSL sediment tube samples are currently being measured by Dr. Sebastien Huot at the University

of Illinois to further calibrate the age of units in the trench. At least one earlier event can be inferred from the presence of scarp-derived colluvium(s). It is not clear whether units 3C and 4C have developed from the same scarp rejuvenation event. In terms of soil features units 4C and 4X appear to have a similar type of soil development, while unit 3 deposits are more similar to unit 2C. Nevertheless, it is reasonable to assume that the penultimate colluvium formed at or since the age that comes from unit 4C, i.e. at or since 1900-2003 cal yr BP.

In summary, despite the lack of evidence for faulting it is possible to interpret that one or possibly 2 scarp-derived colluviums have developed at the site during the last c. 2000 years. Based on the development of paleosol 3a (which represents a significant amount of geologic time) and the charcoal dates, it is reasonable to infer that the best candidate for the most recent faulting-derived colluvium (earthquake event) was at or post-dates c. 1900-2000 cal yr BP. Fire, as implied by the presence of charcoal, could be considered as an alternative agent to cause colluviation or sediment flux.

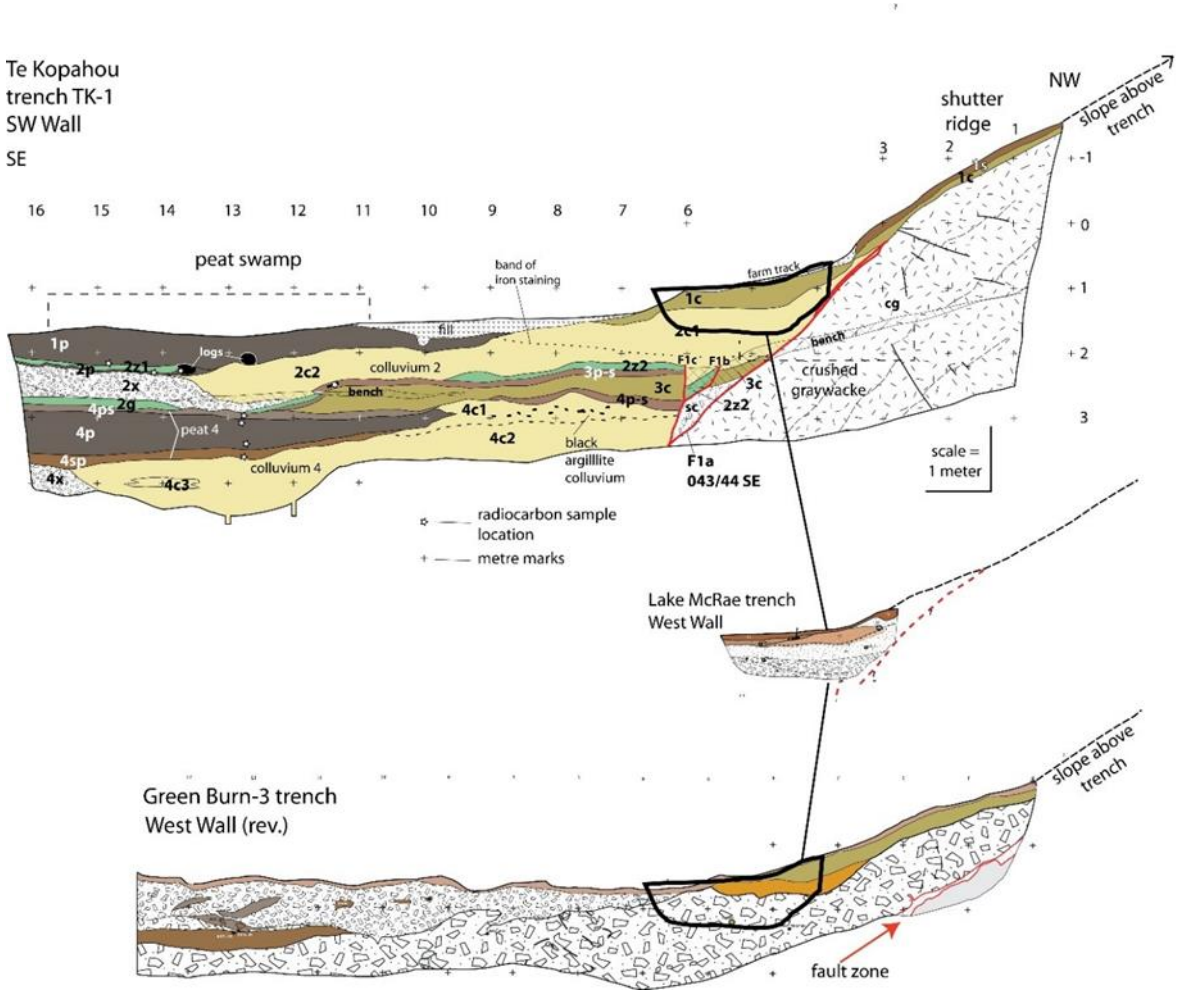

Figure 3.5 Three examples of low-angle faulting associated with strike-slip faults with tall shutter scarps in New Zealand. Top: Te Kopahou-1 trench on the Wellington Fault near Cook Strait. Middle: McRae hand-dug trench. Bottom: The Green Burn-3 trench excavated in 2016 on the Hope Fault. The size and shape of the McRae trench has been superimposed on the other two machine-excavated trenches to illustrate where the fault zone could be relative to the Lake McRae excavation.

Other fault trenches excavated into large shutter ridges across major strike-slip faults in central New Zealand have shown that the faulting can be expressed by a zone of moderate to low dip angle of faulting (Figure 3.5). For example, the Te Kopahou site on the southern end of the Wellington Fault displays a 42° dipping zone of faulting that bounds a greywacke-cored shutter ridge (Langridge et al., 2011). Nutty colluviums inferred to have formed following co-seismic

faulting events can be up to 1 m thick and extend up to 8-9 m from the fault zone. A trench along the Conway segment of the Hope Fault at Green Burn Stream displays a low-angle zone of faulting (30°) adjacent to an 8 m high fault scarp. If we consider the short and shallow nature of a hand-dug trench such as the McRae trench, then it is possible that the zone of faulting could be shallow-dipping and would extend at a low-angle to the north of the trench exposure. In addition, the scale of the Lake McRae trench highlights that it would be easy to over-interpret the record there based on the number of mapped units in a 70 cm deep trench versus other sites.

4.0 LANDSLIDE INVESTIGATIONS

4.1 INTRODUCTION

A major goal of this study is to determine the age of Lake McRae through investigations of both the landslides and the sedimentary fill of the lake. To assess the age and structure of the two large landslides that dam Lake McRae, we mapped the landslides and their runout debris deposits and looked for exposures or exposed boulders within the landslide debris which could be sampled for age determination (see Figure 4.1, Figure 4.2). No exposures were found, therefore we focused on collecting rock samples from sites on landslide LS1 for cosmogenic dating.

4.2 LANDSLIDE MAPPING

Mapping of landslide LS1 indicated that a large debris avalanche had fallen from the steep rock slopes to the north of the lake. The headscarp walls are typically steep with slopes of c. 28°. The arcuate headscarp is c. 0.75 km wide and is formed within highly fractured greywacke bedrock forming the northern mountain rangefront. The main avalanche deposit forms an area of raised, undulating topography at the toe of the slope which had runout a significant distance across the valley before terminating at the base of the slope from the southern valley (Figure 4.1). The LS1 deposit occurs at the west end of the lake and has a surface area (including beneath the lake) of c. 0.53 km^2. The deposit was generally covered with low-lying shrub vegetation and comprised of a mixture medium to coarse grained material with occasional large boulders which protruded from the surrounding ground surface.

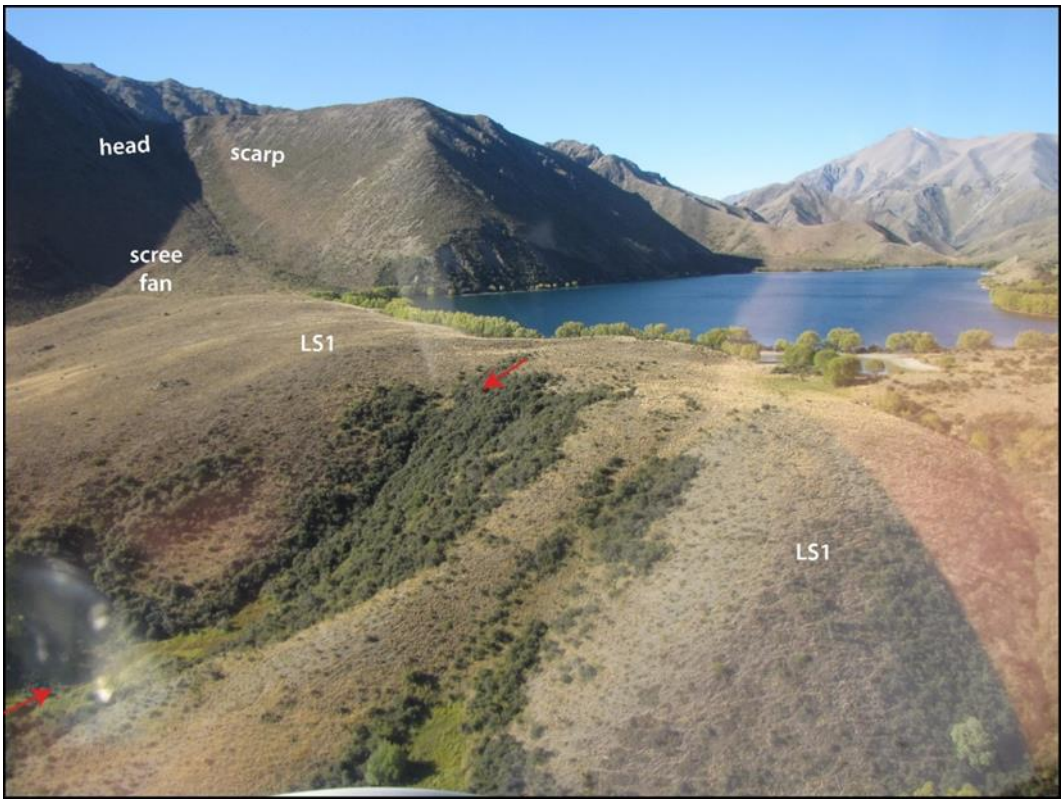

Figure 4.1 The LS1 landslide deposit occurs in the foreground impounding Lake McRae. The source area of LS1 is at upper left, partially in shadow. The trace of the Clarence Fault cutting LS1 is identified by springs and the green vegetation at lower left (red arrows).

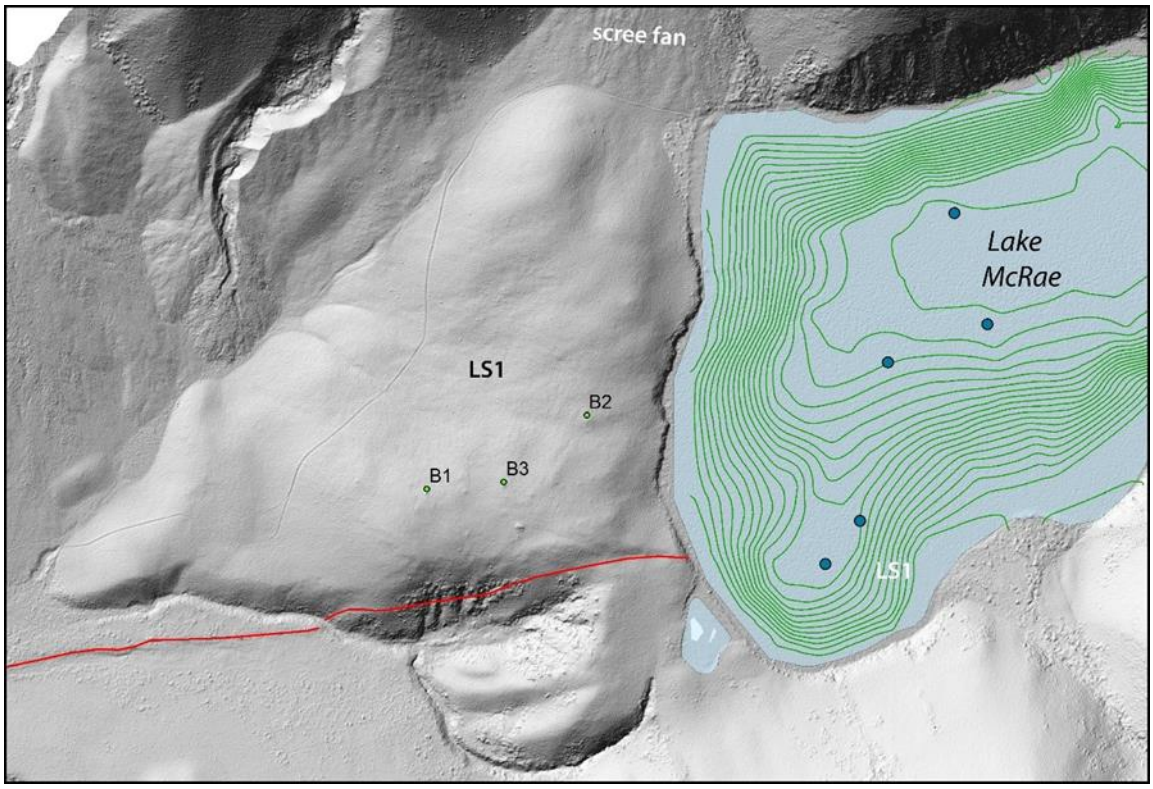

Figure 4.2 LiDAR hillshade model of the LS1 landslide deposit at the west end of Lake McRae. Samples for cosmogenic dating were collected at sites B1 to B3. Red line represents the mapped trace of the Clarence Fault cutting and west of LS1. Bathymetric contour interval is 2 m. Lobes within the bathymetry of the western part of the lake highlight the sub-lake continuation of LS1. Core sites are shown by blue circles.

To estimate the volume of landslide LS1 we estimated the average thickness of the landslide above the level of the lake (30 m; times the area) and added to that the estimated volume of the landslide beneath the lake and filling the valley (Figure 4.2). The former is c. 16 x 10^6 m^3 and the latter, based on a valley depth of c. 50 m (i.e. the depth of the lake plus the sediment thickness) is c. 25 x 10^6 m^3, for a total of c. 41 x 10^6 m^3. According to the global classification of subaerial landslides by Cruden and Varnes (1996) (see Hancox and Perrin, 2009), LS1 can be classified as a 'very large' landslide.

Landslide LS2 is located at the east end of the lake and has a surface area (including beneath the lake) of c. 0.75 km^2. To estimate the volume of landslide LS2 we sub-divided the landslide into four areas for which we derived volumes, both below and above the level of the lake. This yields a volume of c. 70 x 10^6 m^3 which also results in a 'very large' landslide classification. The large embayment in the north end of LS2 (Figure 4.3) probably represents a secondary failure of the frontal portion of LS2 (see Chapter 5 for a description of the bathymetry and morphometry of this area).

Figure 4.3 Aerial photo of the upper part of the LS2 landslide deposit, looking back to the South toward the source area. The upper part of the deposit is characteristically very hummocky.

4.3 COSMOGENIC DATING OF LARGE LANDSLIDE DEPOSITS

4.3.1 Introduction

Cosmogenic dating is the use of cosmic-ray produced isotopes to determine the age of a geologic sample (for this study an event) that has caused a surface to become (partially) exposed to open sky. A great number of isotopes are produced at the Earth's surface through nuclear reactions between cosmic-ray particles (mostly secondary neutrons) and target atoms of exposed surfaces. But only a few of them (e.g. ^{3}He, ^{10}Be, ^{26}Al, ^{36}Cl) have natural abundances low enough for the cosmogenic fingerprint to be quantifiable. This 'cosmogenic clock' starts at the onset of exposure. The technique was developed several decades ago and is widely used (Gosse and Phillips, 2001; Dunai, 2010).

One key aspect of this technique, which is unique from other dating techniques (e.g. radiocarbon dating), is that longer exposed surfaces have a higher concentration of the cosmogenic isotope. Thus very recently exposed surfaces have very low concentrations of such isotopes, whilst much older surfaces have higher concentration making them easier to date. The accuracy of the method, however, depends on the assumption that at the time of exposure associated with an event the surface has a zero concentration (zero inheritance) of the cosmogenic isotope. The validity of this assumption for the surfaces sampled in this study will be discussed in more detail in section 4.3.7.

The simplest and most frequently used analytical approach is to determine the concentration of beryllium-10 in quartz grains extracted from sampled rock surfaces and to convert ^{10}Be concentration values to exposure ages using a commonly used calibration scheme implemented through the web-enabled CRONUS calculator (Balco et al., 2008).

4.3.2 Sample Selection

Landslides LS1 and LS2 were considered for cosmogenic dating. Only one appropriate protruding rock/ boulder was observed during reconnaissance of LS2. LS1, however, had multiple rocky tors and boulders protruding from its surface and as consequence was the site focused on for dating.

To determine the age of landslide LS1, three tors/boulders (B1, B2, B3) were selected and sampled for cosmogenic dating, see Figure 4.3, Figure 4.4, and Figure 4.5. The approximate geographical location, necessary for production rate calibration, is the same for all four samples from these the three boulders: -42.2°N, 173.3°E, 920 m a.s.l. The main selection criteria for choosing these locations were the size and height of the tor above surrounding soil and their distance from the landslide headscarp. Generally, the larger boulders were considered less likely to have been subject to post-depositional movement and boulders toward the lower section of the deposit could not have been deposited after the large rock avalanche event. The present-day orientation of the exposed surface relative to zenith is taken into account when calculating the exposure age, making the implicit assumption that that orientation has not changed significantly over the exposure period.

Figure 4.4 The LS1 landslide deposit, looking back to the North toward the source area and scree fan. The line in the mid-ground is the crest of the deposit above the lake. Hard, rocky tors and boulders of greywacke sandstone (LS1-B1 sample area) stick out of the landslide mass and were targets for cosmogenic dating samples.

From the top of these boulders a section of rock 2-5 cm deep was removed using a battery powered angle grinder and with a hammer and chisel, see Figure 4.5, resulting in 1.5-2.5 kg samples of 2-5 cm fragments, see Table 4.1. From boulder B1 one additional sample of rock was taken by removing it as one lump (sample S2, approx. spherical, ~15 cm diameter, ~2 kg).

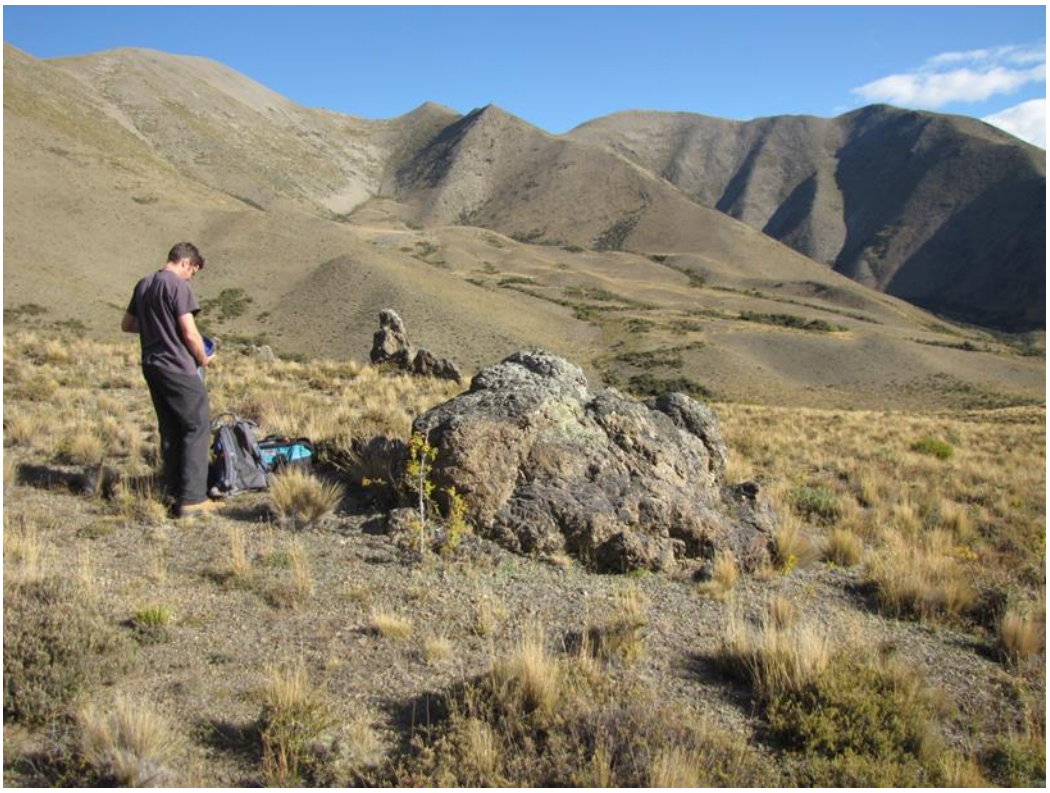

Figure 4.5 Two rocky greywacke tors extending out of the LS1 landslide deposit. Cosmogenic sample LS1-B3 came from this exposure. Landscapes in the distance are also affected by landsliding.

Figure 4.6 Rock sampling technique on the LS1 landslide deposit. A square area of north-facing surface rock was prised out with a portable rocksaw and manually with a hammer and chisel (sample LS1-B3).

4.3.3 Physical and Chemical Preparation

At the National Isotope Centre (NIC), the samples were crushed with a pneumatic press and roller mill and then sieved to select the particle size fraction smaller than 0.5 mm, see Table 4.3.2. Because of a lack of information about the exact location of sample S2 on boulder B1 and resulting uncertainty about its exposure geometry, its shielding parameters were regarded to be equal to that of S1 from the same boulder. For that reason, the whole of S2 was broken into smaller pieces and treated like the other three samples. Only a fraction of available sample was necessary for processing, with remaining amounts of raw rock and crushed material put into archive. Hot phosphoric acid (HPA) was used to extract the quartz component. A new procedure and new equipment have been developed in-house to make this method effective, efficient, and safe (Ditchburn et al., 2014). Compared to the more commonly applied technique of etching with hydrofluoric acid (Kohl and Nishiizumi, 1992), the main benefit of the HPA-based procedure is higher selectivity in dissolving silica-based compounds while leaving quartz grains largely intact. From each sample, two amounts of 200-250 g of rock were processed with the HPA method and the resulting quartz was combined afterwards, see Table 4.2. On average, 13% of the greywacke rock was extracted as quartz.

Samples were then processed by the cosmo-sample preparation laboratory at VUW for Be carrier addition, dissolution, and Be separation via ion-exchange chromatography. Within each testing batch of 10 samples, at least one processing blank is run as a control. The resulting Be hydroxide gels were then returned to NIC for oxidisation to BeO and subsequent addition of silver powder (ca. 1:1 by volume) to make the sample electrically conductive. The oxidisation procedure involves a two-step conversion: from the hydroxide to the sulphate form by the addition of sulphuric and hydrofluoric acids, and then to the oxide by breaking the sulphate using high heat. HF is introduced in the first step to drive off boron as BF_3 gas, as too much boron-10 in the BeO sample impedes proper detection of ^{10}Be atoms during AMS measurement.

4.3.4 ^{10}Be AMS Measurement

Approximately 1 mg BeO+Ag sample mixtures are loaded and pressed in NEC-type cathode holders made out of oxygen-free copper. ^{10}Be/^{9}Be measurements (wheel BeW186) were made with the XCAMS system at NIC, using an effective technique to reject any remaining boron-10 coming through with the ^{10}Be beam towards the particle detector (Zondervan et al. 2015). The system's calibration is determined by concurrent measurement of internationally accepted standards from UC-Berkeley (Nishiizumi et al., 2007). Likewise, the system background count rate is assessed with a several 'machine' blanks prepared from a Be carrier that has a ^{10}Be/^{9}Be ratio well below the detection limit of XCAMS. Measurement data are analysed offline for outliers, summarised, background-corrected, and calibrated to absolute isotopic abundance ratios (^{10}Be atoms) / (^{9}Be atoms), see Table 4.3. Subsequently, the processing blank in terms of 10Be atoms is subtracted and final results are expressed as ^{10}Be concentrations and their associated measurement uncertainty.

4.3.5 Exposure Age Calculation

Exposure ages are derived with the CRONUS calculator (Balco et al., 2008), using the following pertinent sample parameters: geographic location, topography of surrounding hills, thickness, strike, and dip of the sampled surface layer, ^{10}Be concentration in quartz, and its associated analytical error. For each input record of sample information, this calculator returns a number of exposure ages, one for each production rate calibration scheme. The differences amongst these schemes are rather subtle and their discussion is beyond the scope of this

study. For further information about the schemes, see the references on the CRONUS calculator website (Balco et al., 2008).

Table 4.1 Parameters associated with sampling the rock surfaces from the boulders / tors on landslide LS1.

Sample field ID	depth (cm)	strike direction (°)	dip angle (°)	topographic shielding factor	# rock fragments	weight (kg)
L1B3S1	2	125	11	0.972	many small	> 2
L1B2S1	1.5	116	0	0.973	many small	1.9
L1B1S1	1.5	90	15	0.976	many small	1.5
L1B1S2	1.5	not determined	not determined	0.976	one large	> 2

Table 4.2 Parameters associated with AMS sample preparation.

Sample field ID	NIC lab ID	rock processed (g)	quartz extracted (g)	VUW lab ID	quartz dissolved (g)	Be carrier added (mg)
L1B3S1	TCN1	467	59.4	KV284	39.7	0.368
L1B2S1	TCN2	471	67.3	KV285	51.5	0.366
L1B1S1	TCN3	455	57	KV286	45.7	0.367
L1B1S2	TCN4	428	61.5	KV287	44.8	0.366
				KV288 proc-blank	0	0.399

Table 4.3 Parameters associated with AMS sample measurement.

VUW lab ID	Be#	10Be/9Be (at/at)	error (at/at)	10Be (at)	error (at)	net 10Be (at)	error (at)
KV284	3759	2.38E-13	9E-15	5.9E+06	2E+05	5.6E+06	2E+05
KV285	3760	3.67E-13	1.4E-14	9.0E+06	3E+05	8.7E+06	3E+05
KV286	3761	2.47E-13	1.0E-14	6.0E+06	3E+05	5.8E+06	3E+05
KV287	3762	2.47E-13	1.0E-14	6.0E+06	2E+05	5.8E+06	2E+05
KV288 proc-blank	3763	9.9E-15	1.6E-15	2.6E+05	4E+04	0 (by definition)	

Table 4.4 Parameters associated with converting ^{10}Be concentrations to exposure ages.

Sample field ID	10Be conc. (at/g)	error (at/g)	total shielding factor	analytical error (ka)	exposure age (ka)	total error (ka)
L1B3S1	1.41E+05	6E+03	0.972	713	16793	1719
L1B2S1	1.69E+05	7E+03	0.973	781	20072	2026
L1B1S1	1.26E+05	6E+03	0.976	658	14911	1537
L1B1S2	1.29E+05	5E+03	0.976	630	15211	1551

4.3.6 Results

We present in Table 4.4 all cosmogenic data for the three boulders from landslide LS1. The shielding correction calculations show that the dip of the sampled surface is too small to influence the total shielding and that the latter is totally governed by cosmic-ray shielding by surrounding hills. The density of rock was assumed to be 2.65 g/cm^3. The rate of surface erosion was assumed to be negligible and thus set to zero. Rather than presenting all results put out by the CRONUS calculator, we show only the results for the time-dependent Lal-Stone scheme (Balco et al., 2008 and references therein). Two types of uncertainty on the exposure age are given in Table 4.4: the analytical error and the total error. The latter is a combination of the analytical error and the model error, thereby capturing all known sources of uncertainty. When inter-comparing multiple samples from the same site and associated with the same exposure event, for example to test repeatability, one should use the analytical error only and treat it as a random error, i.e. of statistical nature. The total error on the other hand needs to be used to estimate the uncertainty of the exposure age. The model error is a property of the selected calibration scheme and is of systematic nature: It cannot be reduced by more repeat measurements of the same boulder.

4.3.7 Discussion

Figure 4.7 is a plot of probability distributions (a.k.a. probability density functions, PDFs) for the measured exposure ages. The width of each distribution is determined by the associated analytical error. Clearly, the results show a significant degree of ambiguity if all three boulders were actually deposited by the same landslide forming LS1. Only two PDFs clearly overlap; They belong to boulder B1. Also, these two have some overlap with the PDF for boulder B3.

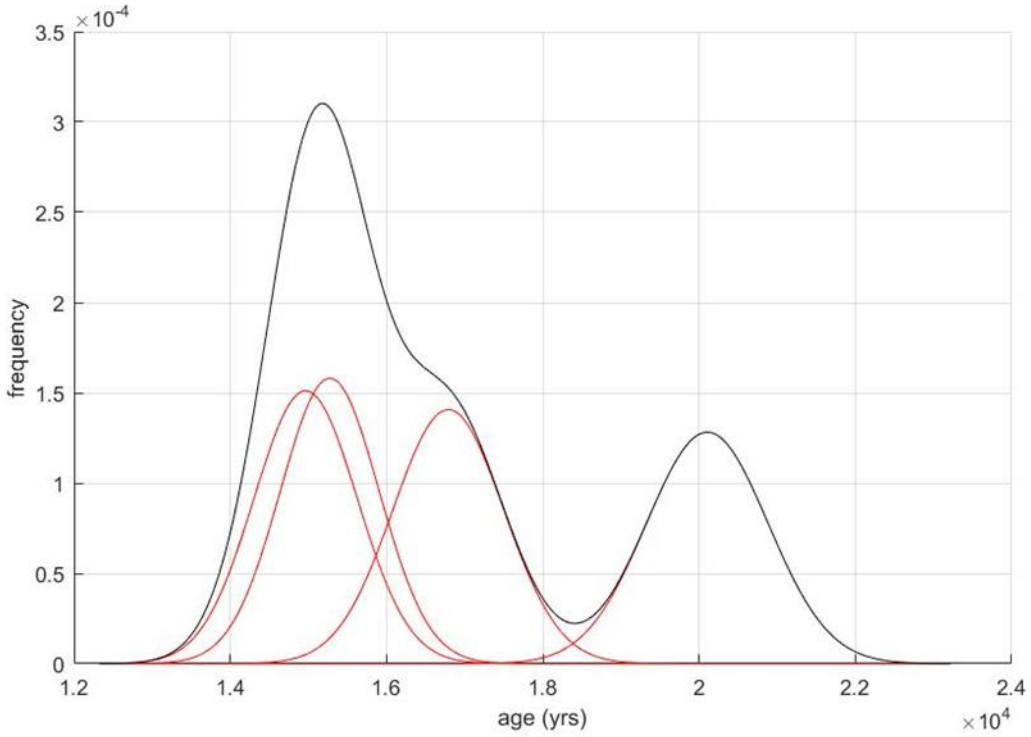

Figure 4.7 Probability density function or camelplot showing the distribution of cosmogenic 10Be ages from rock samples. LS1-B1 (two red curves at left), LS1-B3 (centred on 17,000 yr), and LS1-B2 centred on 20,000 yr. The preferred age of LS1 comes from the shouldered peak derived from LS1-B1 and -B3.

Individual Gaussian PDFs can be combined into one non-Gaussian PDF for the whole set of results, giving an age of $15{,}200^{+3800}_{-2700}$ years as shown in Figure 4.7.

As mentioned above, correct application of the surface exposure dating method is reliant on the correctness of some basic assumptions. The apparent discrepancy between the age of boulder B2 on the one hand and the set of concordant ages for boulders B1 and B3 forces us to consider the validity of these assumptions. Apart from possible issues with the analytical procedures followed, bias towards older ages is most often due to ^{10}Be inherited from exposure during the period leading up to the exposure event. In the setting of this study, we should consider the possibility that boulder B2 was positioned near the surface of the slope before failure. The 1/e attenuation coefficient for those cosmic rays that produce ^{10}Be is c. 0.65 m. Therefore, only several thousand years of pre-landslide exposure of the sampled surface would be required to bias the event age from the true age further back in time by a similar amount. Obviously, the degree of bias depends on how deep and how long the boulder was located within the hill before failure. Possibly, gradual erosion of the hill slope before the landslide slowly brought boulder B2 closer to the surface, allowing the cosmogenic clock to start before the landslide event we wish to date.

Bias towards younger ^{10}Be ages can be achieved by underestimating the rate of erosion and/or the degree of shielding. In the CRONUS calculations presented so far we assumed that the sampled surfaces have not eroded at all since the start of the exposure. If, however, we assume a 15 mm/ka erosion rate for boulders B1 and B3 while maintaining a zero erosion rate for B2, then the (average) exposure age for B1 and B3 increases to that of boulder B2. This exercise demonstrates that the sampled boulders must have eroded at significantly different rates to explain the incongruence in exposure ages as shown in Table 4.4. This raises the question if other parameters support or discount that scenario. It also shows an opportunity to use *in situ* produced ^{14}C, to better constrain the exposure age by leveraging its short radiometric half-life. Generally speaking, the two-isotope approach provides in some settings a much more informative result than a single-isotope analysis: The longer-lived isotope (e.g. ^{10}Be) yields the best constraint for the exposure age, while the younger-lived isotope (e.g. ^{14}C, ^{26}Al) best determines the rate of erosion (Goehring et al., 2013). Underestimation of shielding is unlikely with these precautions satisfied:

- Samples were taken from (near) the top of the boulder
- The boulder is large and firmly grounded in surrounding rock or soil
- Data were gathered on horizon topography to account for shielding of cosmic rays by surrounding hills and on sample orientation to account for shielding by rock close to the sampled surface.

It appears these conditions were satisfied in this study.

Finally, we must consider the possibility that boulder B2 was deposited at its current location ca. 4 ka before boulders B1 and B3. Our field survey and Lidar observations suggest there is no major difference amongst the locations of these boulders and therefore does not support the scenario of two landslides well separated in time.

4.3.8 Summary

Cosmogenic dating of greywacke sandstone from rocks and tors on landslide deposit LS1 yields an age of $15{,}200^{+3800}_{-2700}$. This age is consistent with the end of the last glacial period.

5.0 INVESTIGATIONS WITHIN LAKE MCRAE

To assess the geological history of Lake McRae we undertook a small boat campaign to acquire: (i) bathymetry of the lake floor; (ii) shallow seismic sections of the lacustrine stratigraphy in order to understand the sub-structure of the lake and to select core sites; and (iii) shallow cores of the lacustrine sediment.

Figure 5.1 Inflatable boats used to survey and core within Lake McRae. The lake has a maximum depth of c. 43 m. The trace of the Clarence Fault is seen by the green vegetation line behind the boat.

5.1 METHODS

5.1.1 Site Survey

11.6 km of geophysical lines were collected on a grid to map the bathymetry and image the subsurface sediments of the lake. Geophysical data was collected in 2015 using a Knudsen 3.5 kHz central frequency Compressed High-intensity Radar Pulse (CHIRP). A handheld Global Positioning System (GPS) unit provided positional information for each ping to an accuracy of ±4 m. Raw data were processed using a band pass and automatic gain control filters in Globe Claritas software, and imported into Paradigm software for visualisation, mapping and interpretation of the subsurface sedimentary features of the lakes. Bathymetry for the lake was produced in ArcMap using the nearest neighbour algorithm to convert picks of the sediment water interface on the geophysical lines into a bathymetry raster (Figure 5.2).

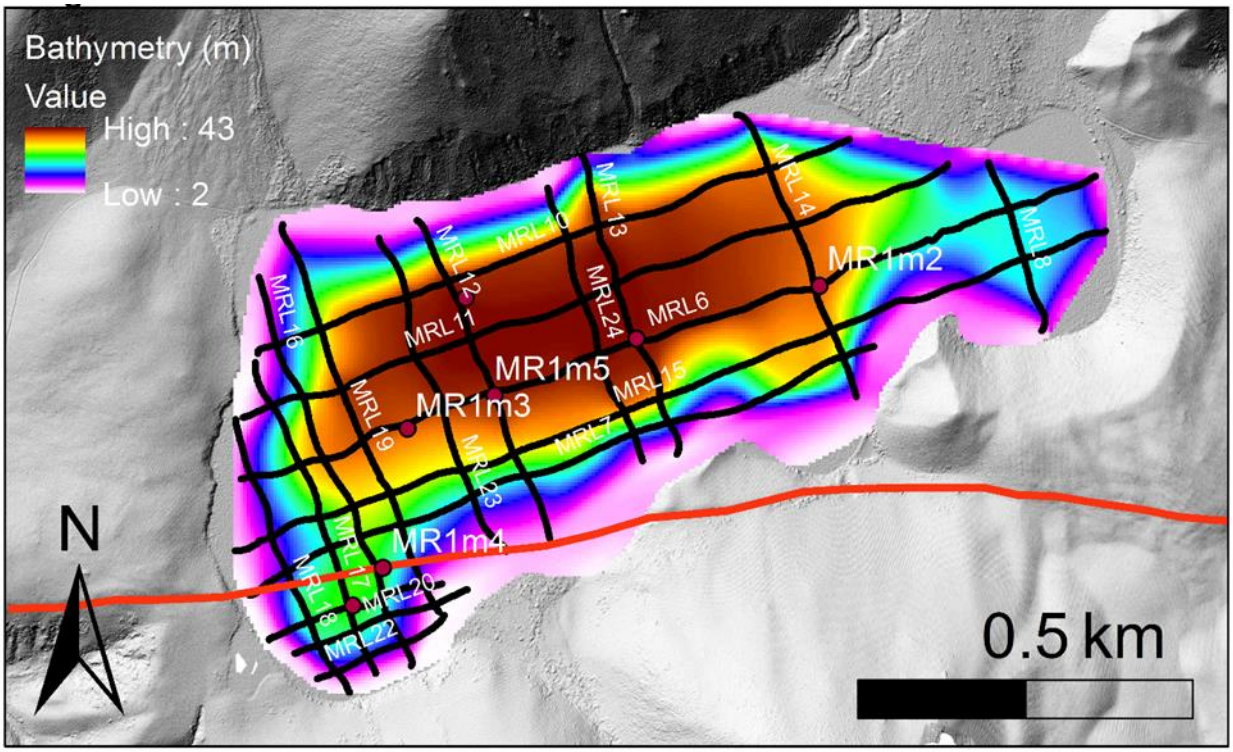

Figure 5.2 Bathymetric map of Lake McRae based on the GHRIP survey. The map shows the core and geophysical line locations.

5.1.2 Sedimentology

Seven 1 m long sediment cores, were collected from along the depocentral axis of Lake McRae using a mini Mackereth corer (Mackereth, 1958). The cores were line-scan imaged, and their physical properties, including gamma density, magnetic susceptibility and colour spectrometry, were characterised using a GEOTEK™ multi sensor core logger. Visual core logs and the physical properties data were used to correlate the cores and to identify different types of deposit in the sediment record. Sedimentary deposits were further characterised using grain-size and spectrophotometry.

Grainsize analysis was conducted on core MR1m5. The deposits were sub-sampled at 2.5 mm resolution and treated with 5 ml of 30% H_2O_2 at 50º C for 12 hours to remove organic matter. Biogenic silica was removed using 10 ml of 1 M NaOH and heating to 50 ºC for 4 hours, shaking for 30 minutes and reheating to 50º C for 30 minutes. Samples were deflocculated using 5 ml of 5% sodium hexametaphosphate solution and shaken for two hours. After deflocculation, grainsize was analysed on a Malvern Mastersizer 2000G laser diffraction particle size analyser coupled to a HydroG dispersion unit.

Spectrophotometry was carried out using a Minolta 2600d spectrophotometer that measures sediment colour in reflectance wavelengths from 365-745 nm at 5 mm resolution down-core. The shape of first-derivative reflectance spectra (FDS) was used to distinguish different pigments linked to organic matter degradation and clay content. For example, in the 600-700 nm band unmodified organic matter can be distinguished from highly degraded organic matter by the presence of Chlorophyll-a signature (Figure 3.1; Debrets et al., 2011; Sebag et al., 2013). Highly degraded organic matter is indicative of allochthonous sources, while Chlorophyll-a is more commonly associated with autochthonous organic material.

5.1.3 Chronology

Chronology for the sedimentary record of Lake McRae is based on AMS radiocarbon dates from terrestrial macrofossils extracted from hemipelagic sediments of three different cores. The dated macrofossils included a twig macrofossil from 55.3 cm core on MA1m2, bark of an unknown taxa from a depth of 38.5 cm on MA1m5, and a twig macrofossil from a depth of 64 cm on core MR1m6. Core MA1m5 was selected as the master core for producing an age model and the equivalent depths on MR1m5 for each date were determined using core to core correlations based on physical properties and distinct sedimentary layers (Figure 5.5). Macrofossils cleaned of residual sediment were subjected to a standard A-A-A (acid-alkali-acid) pre-treatment procedure to remove carbonates, fulvic compounds and humic compounds (cf. Hua et al., 2001). The pre-treated macrofossils were converted to CO2 by combustion, graphitized and measured by Accelerator Mass Spectrometry (AMS) (cf. Baisden et al. 2013) at Rafter Radiocarbon Laboratory. Age models were then produced for the upper 50 cm of the MR1m5 using the P_sequence Bayesian age depth model in OxCal 4.2 with a variable event thickness constant (Bronk Ramsey and Lee, 2012).

5.2 Results and Discussion

5.2.1 Bathymetry

The geophysical survey provides the first constraints on the bathymetry of Lake McRae (Figure 5.2). The lake bathymetry is controlled by the subaerial hillslopes and bounding landslides that extend sub-aqueously to a relatively flat lake floor with a maximum depth of 43 m (Figure 5.2). Other notable bathymetric features include the small fault controlled basin in 'Fault Bay' and the shelf at the eastern margin of the lake. The shelf is immediately adjacent to a distinctive arcuate scarp in the landslide deposit that bounds the north eastern margin of the lake. Our interpretation is that the shelf was formed by an intact block slide which nucleated in the landslide deposit.

5.2.2 Deposits and Depositional Processes

Cores from Lake McRae contain two main lithofacies: layered silt and rapidly deposited layers (Table 5.1). Layered silts are characterised by medium to fine silts that are faintly layered at the centimetre scale and are between 1-200 mm thick. They have relatively low density and magnetic susceptibility (Figure 5.3 and Figure 5.5). The first derivative spectra (FDS) of layer silts have a pronounced trough then peak at ~675 nm, indicative of Chlorophyll-a, which is characteristic of sediment organic matter sourced from lacustrine algae (Figure 3.1) Debrets et al., 2014). Layered silt units in cores from the basin margins also contain layers of macro-organic material from macrophyte species. Macrophytes require light for photosynthesis and their position in cores from sites with water depths up to 40 m most likely indicates extremely clear water allowing light to penetrate to such depths. Sufficient water clarity is probably only reached during periods of low allochthonous sediment supply to the lake that would lower the concentrations of particulates in the water column. Combined, the characteristics of layered silts are indicative of sediments formed by gradual settling of sediment from the water column during times of reduced terrigenous flux and increased autochthonous sediment production. They record periods of relative stability in the lakes fluvial catchment and are classified as hemipelagite.

Rapidly deposited layers (RDL) are composed of layers of coarse silt (H1) that normally grade into fine silt (H2) and range in thickness from 3 to 40 mm (Figure 5.3). They have a wedge shaped geometry and are thickest in the core adjacent to the Goat Valley Stream delta. The

organic signal in the FDS of both RDL units is indicative of degraded organic material typical of soils (Figure 5.4, Debrets et al., 2014). RDLs were probably formed by hyperpycnal flows generated by discharge of sediment-laden influent from Goat Valley Stream into the lake because their normal grading suggest deposition from a current, they contain allochthonous organic material and are thickest in cores located close to the major fluvial inflow (Howarth et al., 2014, REFs). They are classified as hyperpycnites.

Table 5.1 Description of facies found in cores from Lake McRae.

Lithofacies	Description	Interpretation
Layered silt	1-100 mm thick beds characterised by medium to fine silt that has relatively high autochthonous organic content.	Formed by gradual accumulation of pelagic and terrestrial sediment.
RDL	Coarse silt that normally grades into fine silt both of which contain terrigenous organic material.	Formed by hyperpycnal flows generated by discharge of sediment laden fluvial effluent.

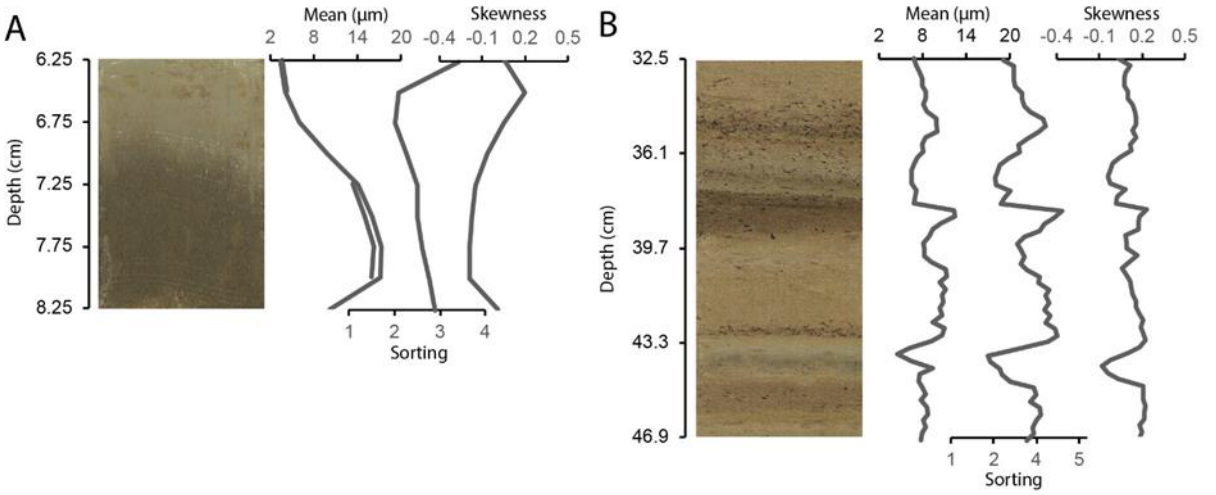

Figure 5.3 Grainsize statistics for representative examples of the rapidly deposited layer (A) and layered silts lithofacies (B). The coarse basal unit of RDL normally grades into the fine upper unit. Layered silts exhibit not clear trend in mean grainsize.

5.2.3 Depositional Architecture

The interpretation of Lake McRae's depositional architecture is informed by both the sediment cores and the geophysical imaging. The stratigraphy of the upper part of the sedimentary fill was determined using the seven ~1 m long sediment cores (Figure 5.5). Peaks and troughs in both density and magnetic susceptibility allow correlation between cores at the decimetre scale, while individual lithofacies facilitate centimetre scale correlations. Magnetic susceptibility and density vary in phase throughout the cores allowing the cores to be subdivided into periods of high and low density and magnetic susceptibility. Phases of high magnetic susceptibility and density are characterised by increases in the relative abundance of the RDL lithofacies. Conversely, phases of low magnetic susceptibility and density are characterised by layered silts. The relationship between the lithofacies and the density and magnetic susceptibility curves shows that the curves provide proxies for the relative importance of allochthonous and autochthonous sedimentation.

The most prominent feature in all the cores is the peak in density and magnetic susceptibility and hence allochthonous sedimentation towards the top of the cores. For example, between 7 cm and 40 cm on core MR1m1 from the basin depocentre (Figure 5.5). This phase of

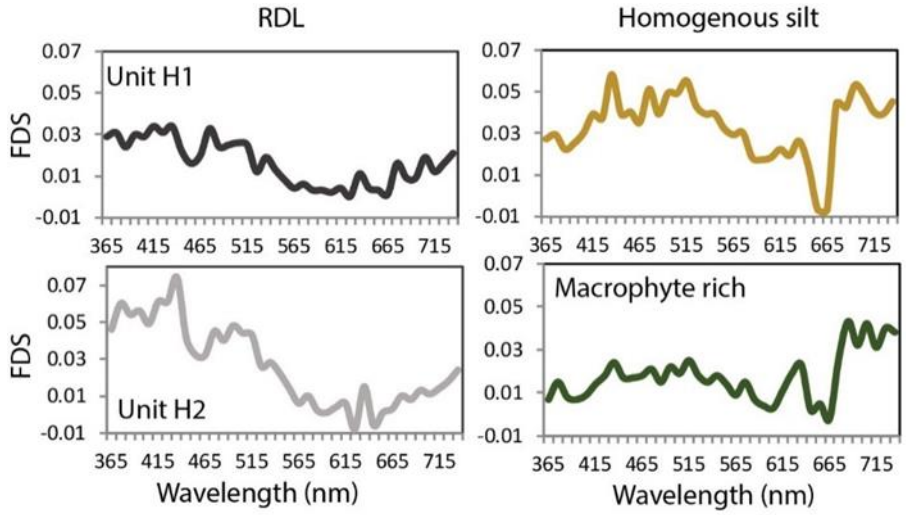

Figure 5.4 First derivative spectra (FDS) for the coarse silt (H1) and fine silt (H2) units of RDL deposits and for layered silt units, both with and without macrophyte content. The spectra between 600 and 700 nm is indicative of the organic matter source. RDL deposits have spectra consistent with degraded organic matter from a detrital source. The layered silts spectra indicate the presence of chlorophyll-a, most probably from lacustrine algae, indicative of an autochthonous source.

allochthonous deposition decreases in thickness with distance from the Goat Valley Stream delta suggesting the stream is the source of the allochthonous sediment. Below this peak the cores are predominantly composed of the layered silt lithofacies and have lower magnetic susceptibility and density indicative of increased importance of autochthonous sedimentation. The abrupt transition to allochthonous sedimentation is consistent with a change in environmental conditions in the Goat Valley Stream catchment resulting in increased sediment supply to channels and the lake. It is not possible to infer the driving mechanism on the basis of the sedimentology alone. Likely causes of the change in sedimentation are discussed in section XX using the chronology to correlate the timing of change to known perturbations. In addition to revealing the detailed stratigraphy of the upper sedimentary fill the cores provide an opportunity to define sedimentation rates that are derived in the following section.

Due to the short extent of the sediment cores (~1 m) the broad scale depositional architecture of the basin is primarily constrained by the geophysical data. Acoustic basement can be observed in the geophysical lines from the southwestern margin of the lake where it is represented by an undulating reflector that dips towards the north east before being obscured by signal attenuation due to the presence of gas or impenetrable sediments (Figure 5.6). The acoustic basement is continuous with the landslide deposit that dams the lake and most likely represents the continuation of the landslide deposit beneath the lake. The landslide deposit is draped by sediments that have a layered acoustic facies and thicken north eastward toward the basin centre and the major sediment source, Goat Valley Stream. They reach a thickness of 15 m at the MR1m5 core site where the basement reflector is last observed. It is not possible to determine the maximum depth of the sedimentary fill in the lake using the geophysical data because the acoustic basement is still dipping to the north east when it is obscured by gas. Never the less the presence of sediments overlying the landslide deposit does allow a minimum age for the landslide to be inferred from sedimentation rate arguments (discussed below).

Within the acoustically layered sediments there are two distinct acoustic facies. The first is characterised by high amplitude reflectors and occurs in the upper part of the sedimentary fill. The second is characterised by relatively low amplitude reflectors and occurs in the lower part of the fill (Figure 5.6). Reflector amplitude is primarily related to the density contrast between sediment layers, whereby high amplitude reflectors represent large contrasts in density. Such density contrasts are most likely to occur where there are significant changes in grainsize or the relative abundance of autochthonous and allochthonous sediments. It follows that the low amplitude acoustic facies contains more homogenous sediments. These acoustic facies preferentially thicken towards the depocentre and Goat Valley Stream. For example, at the intercept of lines 19 and 6 at the distal end of the basin the low amplitude acoustic facies represents only 38% of the sediment pile but increases to 52% at the intersections of lines 12 and 6 (Figure 5.6). The preferential thickening is probably caused by an increase in the abundance of RDL deposited during hyperpycnal flows that preferentially deposit sediments in the depocentre, thin with distance from the delta of Goat Valley Stream and are absent from drape deposits in the distal parts of the basin. Consequently, the low amplitude acoustic facies at the base of the sequence is interpreted to represent a period of predominantly allochthonous sedimentation.

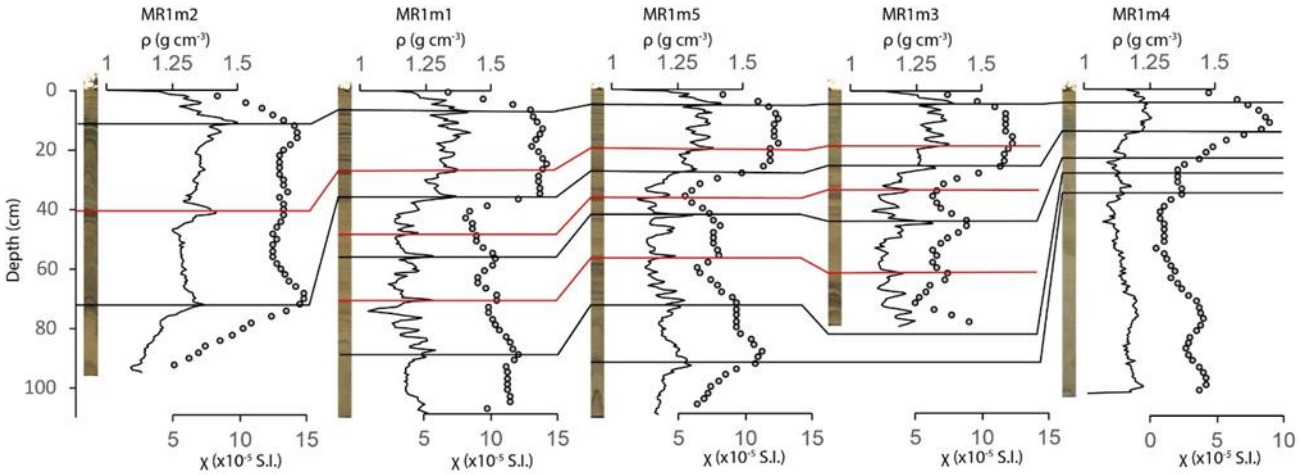

Figure 5.5 Correlations between cores from Lake McRae. Core images, density (p) and magnetic susceptibility (χ) and displayed. Black lines represent correlation between cores based on physical properties data and red lines are correlations based on lithostratigraphy.

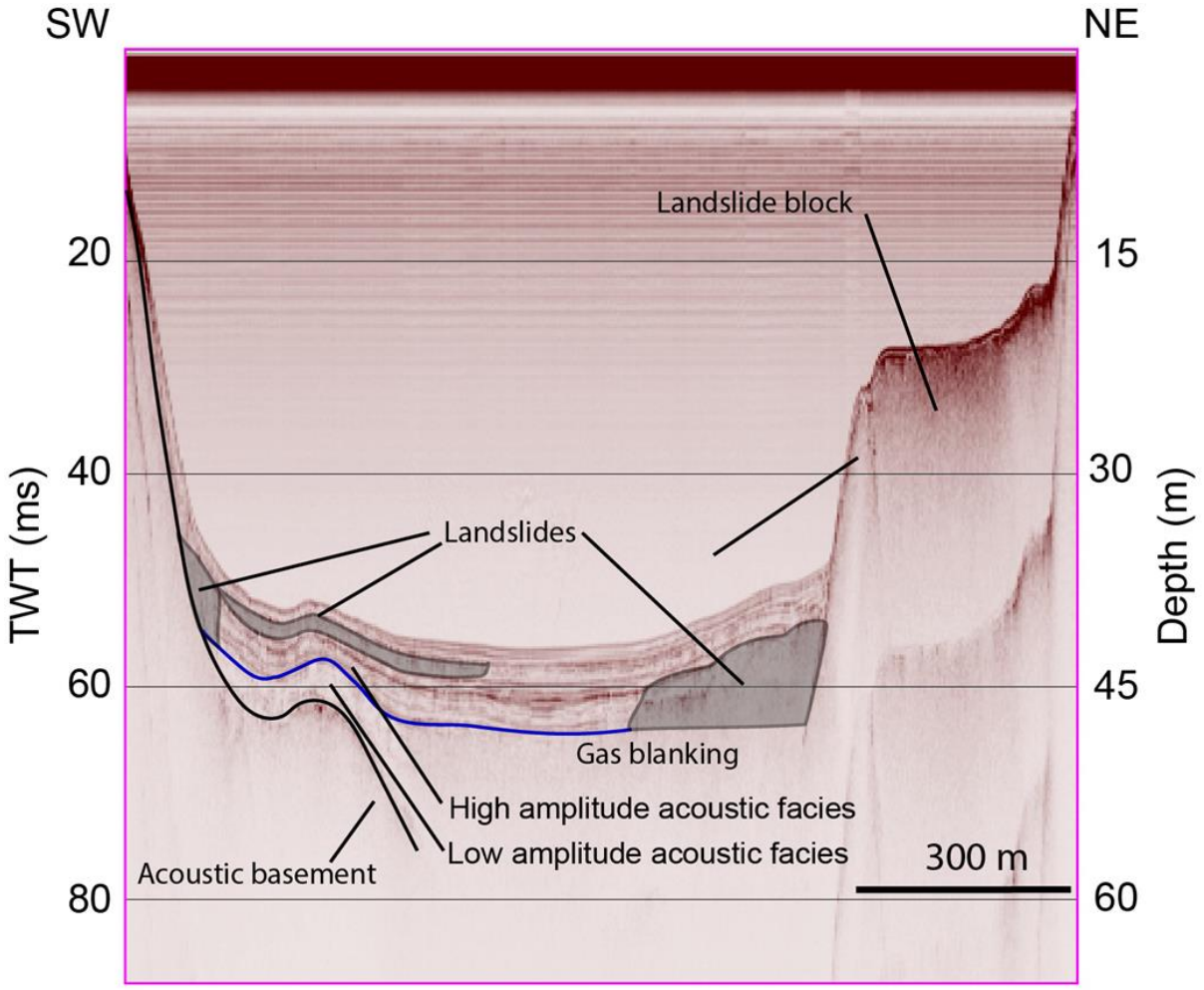

Figure 5.6 CHIRP line MR6 from southwest to northeast along the long axis of the lake basin. The line clearly shows the acoustic basement/damming landslide deposit (LS1), two acoustic facies of lacustrine sediments, large subaqueous landslide deposits, and the landslide block that forms the bathymetric shelf in the northeast of the basin.

The geophysical data also provides evidence for the location of the Clarence fault where it transects the lake and at least one paleoearthquake (Figure 5.7). Multiple fault strands can be seen offsetting acoustic basement and reflectors in the lacustrine sediments on line 16 where a component of dip slip motion has formed a small fault controlled basin. Total vertical displacement on the major fault strand is ~1.4 m. Above the displaced acoustics basement high amplitude reflectors are warped into and then displaced across the fault and the fault tip is draped by un-faulted reflectors. The presence of faulted then un-faulted reflectors indicates the occurrence of surface rupture during an earthquake. A ponded deposit has formed between the faulted and un-faulted reflectors. The geometry of this deposit is consistent with those formed by mass-wasting derived turbidites (Chapron et al., 1999; Howarth et al., 2012; Schnellmann et al., 2002; Strasser et al., 2012). A series of seven small sub-aqueous landslides occur at the same stratigraphic level as the fault rupture event (Figure 5.6, Figure 5.7, Figure 5.8). All of these landslides deposits are subtle features in the geophysical data. They are only a few meters thick and appear as zones of chaotic reflectors and over-thickening in the sedimentary sequence (Figure 5.8). Fault displacement and synchronous subaqueous mass-wasting provides strong evidence for the occurrence of at least one paleo-earthquake since lake formation.

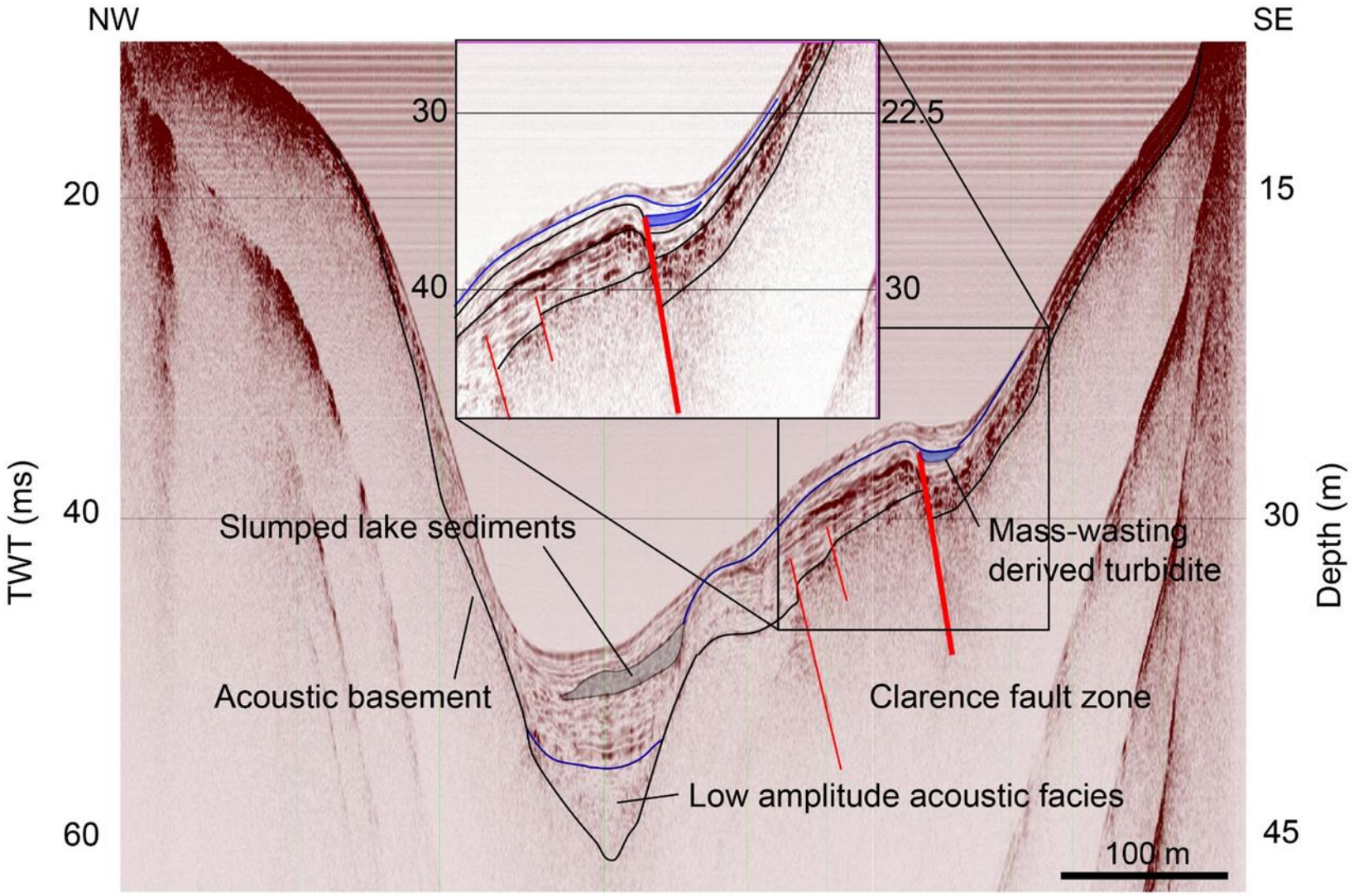

Figure 5.7 CHIRP line MR16 from the north west to south east across the lake basin. This line transects the fault controlled basin in 'Fault Bay' and clearly shows the Clarence Fault zone, evidence for fault rupture and synchronous landsliding in the lake basin.

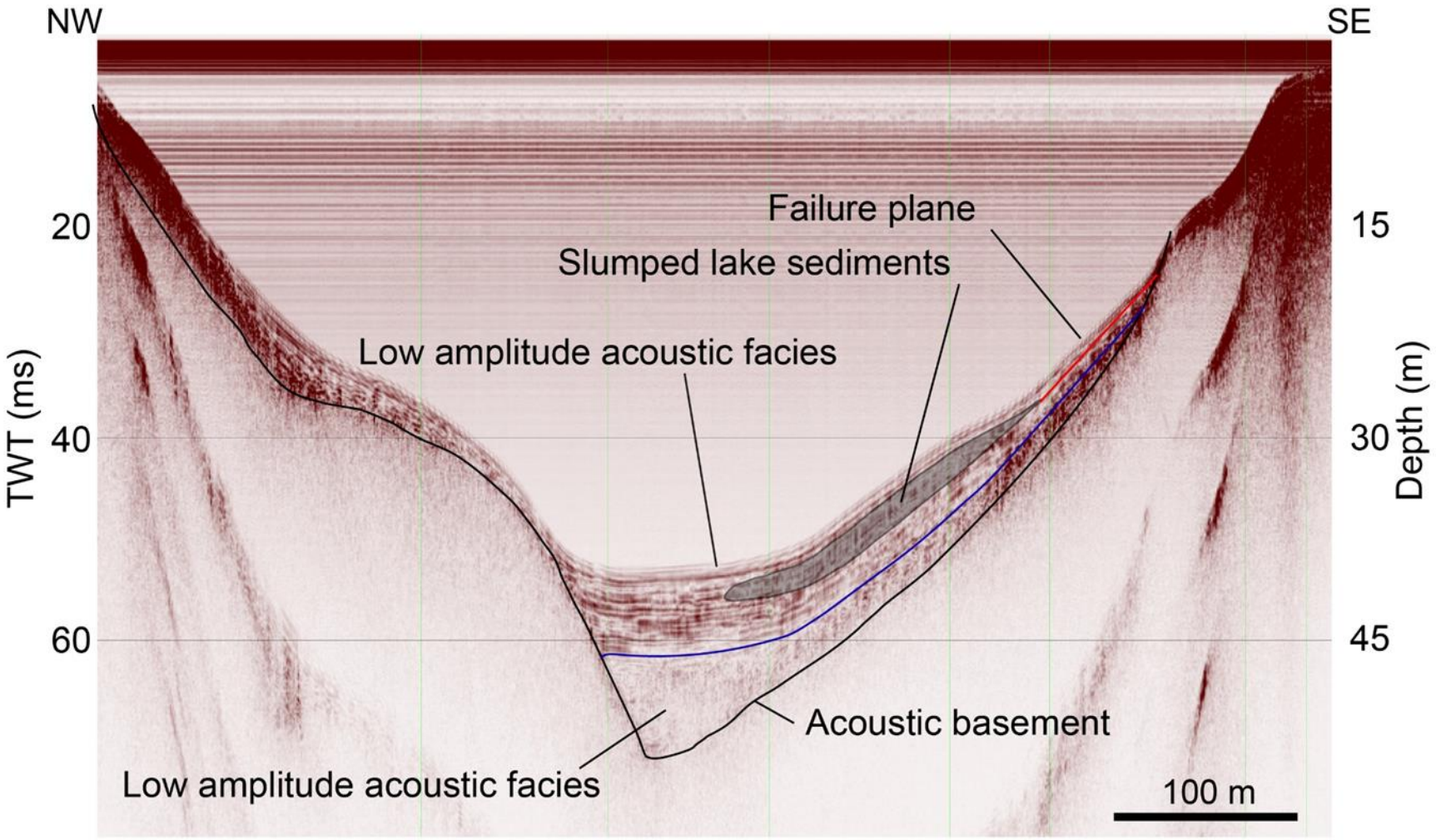

Figure 5.8 CHIRP line MR19 from the northwest to southeast across the lake basin. The line shows an example of the subaqueous mass-wasting that accompanied the last rupture of the Clarence Fault at this location.

5.2.4 Chronology

Chronology was developed on the basis of three radiocarbon dates from terrestrial macrofossil targets (Table 5.2). The P_sequence age model for core MR1m5 was based on these three age constraints and provides a crude chronology for the upper 50 cm of this core that spans the last 350 years (Figure 5.8). The age model also provides an estimate for the timing of the peak in allochthonous sedimentation at the top of the core of 1723 to 1966 A.D. (95% HPDF range). The chronology is also used to generate estimates of sedimentation rate for the lake basin. A sedimentation rate for core MR1m5 was calculated from the interval between 0 cm and 42 cm because the chronostratigraphic marker horizon at 42 cm permits the chronology to be transferred to most of the other core sites, allowing equivalent sedimentation rates to be generated throughout the basin. The 42 cm depth on core MR1m5 has a median age of 1664 A.D. (1541-1793 95% HPDF range) providing an average sedimentation rate of 8.3 yr cm-1 (5.3-11.2 yr cm-1 95% HPDF range) at this core site. Transferring the chronology to the other cores sites shows that sedimentation increases twofold from the lacustrine drape in distal part of the basin to locations close to the Goat Valley Stream delta (Figure 5.3). As core MR1m2 samples only stratigraphy from the upper 35 cm of MR1m5, the peak in allocthonous sedimentation was used as the marker horizon to transfer the chronology. Consequently, the rate for this core is averaged over the last 160 years.

Table 5.2 Radiocarbon dates from Lake McRae used in the age model.

Sample ID	Description	Fraction dated	NZA	CRA [yrBP]	CRA error	$\delta^{13}C$ [‰]	$\delta^{13}C$ error
MR1m2 55.3 cm	Twig macrofossil	Plant material	60339	124	22	-26.1	0.2
MR1m5 38.5 cm	Bark macrofossils	Plant material	60340	253	22	-27.0	0.2
MR1m6 64 cm	Very small twig	Plant material	60341	416	22	-24.6	0.2

Table 5.3 Sediment core sedimentation rates.

Sediment core	Depth to marker horizon (cm)	Mean age (yr)	Age 95% HPDF range	Mean sedimentation rate (yr cm^{-1})	Rate 95% HPDF range
MR1m2	73.2	160	57-304	4.8	0.8-4.2
MR1m1	56.0	350	221-473	6.2	4.0-8.4
MR1m6	49.0	350	221-473	7.2	3.9-8.4
MR1m5	42.0	350	221-473	8.3	5.3-11.2
MR1m3	44.3	350	221-473	7.8	5.0-10.7
MR1m4	31.5	350	221-473	10.9	7.0-15.0

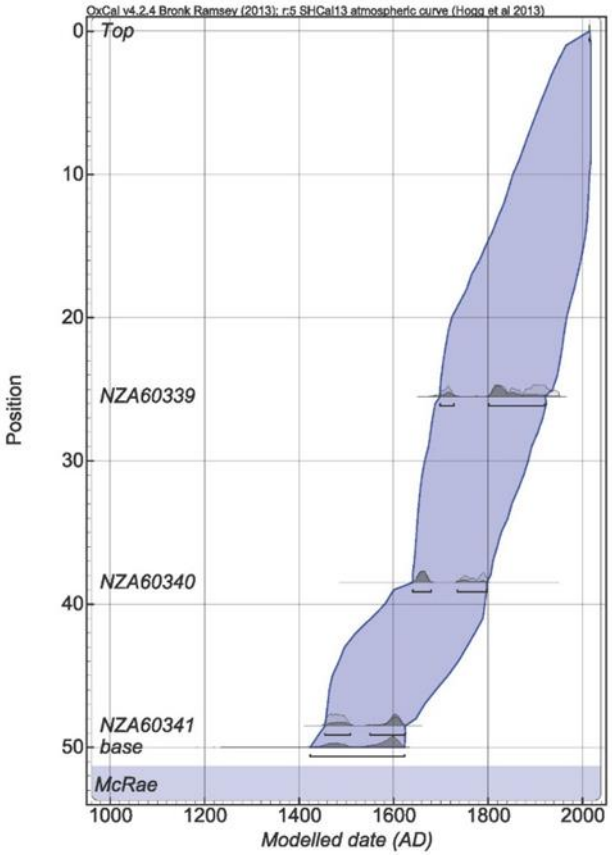

Figure 5.9 Chronological model for Lake McRae based on the upper 50 cm of MR1m5. The age/depth model is based on the radiocarbon dates, the SHCal 13 calibration curve (Hogg et al., 2013) and the P_sequence algorithm in OxCal 4.2 (Bronk Ramsey and Lee, 2013), and shows the calendar age likelihood (light grey) and posterior probability density functions (PDFs) (dark grey), as well as the age models at the 95% level of confidence.

5.3 SUMMARY OF CHRONOSTRATIGRAPHY OF THE LAKE FILL AND PALEOEARTHQUAKE EVIDENCE

The combination of geophysical imaging of the sedimentary fill, and sedimentology and chronology of the lake cores allows a chronostratigraphy to be generated for the events that are observed in the data. The age of the lake bounding landslide can be estimated using sedimentation rate, the depth of sedimentary fill to the landslide deposit at the MR1m5 core site, and the assumption that any changes in sedimentation rate are accounted for by the significant error on the rate. Given that the sedimentation rate includes phases of allochthonous and autochthonous sedimentation and does not take into account compaction of the sediment pile we regard this as a reasonable assumption. The depth of sedimentary fill above the landslide deposit is 15 m at the MR1m4 core site. Based on the sedimentation rate argument the mean age for the landslide is 12,500 cal yr BP and the 95% HPDF age range is 7900-16,900 cal yr BP. This in broad agreement with the ages for the landslide ($15{,}200^{+3800}_{-2700}$ yr BP) derived from exposure age dating. It also suggests that the anomalously old age determination from boulder B2 could be due to inherited ^{10}Be concentrations from pre-failure exposure of the boulder when it was part of the hillslope.

The post glacial age for the landslide is consistent with the change in acoustic facies from low to high amplitude continuous reflectors that we interpret to represent a transition from predominantly allochthonous sedimentation to a combination of allochthonous and autochthonous deposition. Similar transitions are observed in geophysical imaging of

lacustrine sedimentary fill of lakes in Switzerland and Chile and date to the transition from postglacial to Holocene sedimentation (Schnellmann et al., 2006; REF).

The combination of geophysical evidence for fault rupture and the geochronology from the sediment cores allows us to place constraint on the timing of the last earthquake on the Clarence Fault at Lake McRae. The mean sedimentation rate for core MR1m4 is 10.9 yr cm^{-1} (7.0-15.0 yr cm-1 95% HPDF range), which provides a way of estimating the age of the earthquake observed in the geophysical data because the core is located in the fault controlled basin in 'Fault Bay' and directly overlies the evidence of a paleoearthquake. Using this sedimentation rate the mean age for the earthquake is 1575 cal yr BP (1012-2166 cal yr BP 95% HPDF range). This age is consistent with the age of the colluvial wedge formed in the fault proximal trench, which provides additional support for late Holocene rupture of the Lake McRae segment of the Clarence Fault. The earthquake age is also coincident with the timing of the most recent earthquake on the eastern Clarence Fault which occurred 1700-1900 cal yr BP (Van Dissen and Nicol, 2009).

The core age model also provides an estimate for the timing of the peak in allochthonous sedimentation at the top of the core of 1866 A.D. (1723 to 1966 A.D 95% HPDF range). Such an increase in sedimentation rate is most likely linked to disturbance of the lakes fluvial catchment promoting higher sediment production and availability. Two potential triggering events correlate to the timing of change recorded in the lake record. In 1846 pastoral farming was first introduced to this part of Marlborough and by 1853 there were 57 large sheep stations in the region including the Lake McRae area. By 1864 pastoralism had been largely abandoned due to the devastating effects of sheep and rabbit grazing and from the effects of burning on the landscape. It would be reasonable to infer the pastoralism would have altered hillslope stability and increased the production of sediment, which is consistent with our observations that sediment flux to the lake increased at this time. Another potential trigger mechanism is the 1848 Marlborough earthquake that produced MM>VIII shaking at the lake site. We suggest that the earthquake is an unlikely source of the increased sediment flux. The threshold shaking intensity for triggering subaqueous slope failures is lower than that for triggering post seismic increases in sediment flux (Howarth et al., 2014; 2016). Consequently, the sedimentary signature of an earthquake generating high shaking intensities is a turbidite deposited by processes associated with subaqueous mass-wasting, overlain by evidence for increases allochthonous sedimentation. No turbidites indicative of subaqueous mass-wasting were identified in the short sediment cores, precluding an earthquake trigger.

6.0 DISCUSSION OF DATASETS

In this section we discuss the results of the project and interpretation using a list of the key goals to assess how well these were answered.

6.1 AGE OF THE VERY LARGE LANDSLIDES

Based on an analysis of four ^{10}Be cosmogenic dates derived from greywacke rock samples protruding from it, the very large LS1 landslide has an age of $15.2^{+3.8}_{-2.7}$ thousand years (Figure 4.7). This value comes from the weighted mean of the three youngest rock samples, two of which come from the analysis of subsets of the same sampled area (L1-B1). A fourth sample (L1-B2) is statistically older than the other three at 20.07 ± 2.03 ka (Table 4.4). We consider it possible that there is an original inheritance to the age of this sample, i.e. the greywacke tor from which it came could have been part of the original rockface in the rangefront to the north of the lake. The consistency of the two L1-B1 analyses gives us some confidence in the dating technique for these rocks and their consistency with sample L1-B3 gives us further confidence that these three samples are mutually consistent within error.

No material was sampled from Landslide LS2. We infer that LS2 is of similar age to LS1. The major difference in geomorphology between the two is the arcuate scar or eroded area a t the northern front of LS2. This was used to consider that LS2 was older. However, it is more likely that this feature was created by failure of the front of LS2. A CHIRP section through the subsurface structure of the lake (Figure 5.6) indicates acoustic basement related to LS1 and LS2drpaed by high and low amplitude acoustic facies. These are almost certainly bedded lake sediments as seen from the stratigraphy of shallow cores. Due to issues such as gas blanking it is difficult to determine whether LS1 and LS2 occur at the same stratigraphic level with respect to the layered acoustic facies that overlie them. However, it is reasonable to assume that they have a similar timing. Figure 5.6 also indicates that a piece of LS2 occurs as a shallow remnant at the eastern end of the lake. What is clear from CHIRP line MR6 is that the remobilisation of the front of LS2 took place near the boundary between the low and high amplitude acoustic facies.

6.2 THE AGE AND ORIGIN OF LAKE MCRAE

There is no doubt that Lake McRae is a landslide-dammed lake and thus its origin and filling post-dates the emplacement of landslides LS1 and LS2. Using the age model and sedimentation rate from the upper metre of lake fill, it is possible to derive a mean age of 12,500 cal yr BP and an age range of 7900-16,900 cal yr BP for the onset of sedimentation in Lake McRae. These ages are consistent with the ^{10}Be cosmogenic dates described above and give an independent test of the timing of formation of the lake (and landslides).

The timing of the origin of the landslides and lake coincides with the transition from the end of the Late Otiran glacial period (c. 45,000-14,500) and the Late-glacial period (14,500-11,700) of Barrell et al. (2011). Using these authors classification this time period also transitions from the Aranuian (<19,000 yr) and Holocene (<11,700 yr) periods. Clearly at this time, climate was evolving from colder conditions of the Last Glacial Maximum (LGM), to warmer climes of the Holocene. During the maximum of the Late Otiran period, the mountainous central Marlborough region was not fully covered in ice, as was much of the Southern Alps region of the South Island (Barrell et al. 2011). In central Marlborough, cirque glaciers existed in the areas of highest topography such as Mt. Giles (Barrell et al., 2011) and Mt. St. Bernard (Figure 1.1). During the LGM moderate height mountains such as those that surround Lake McRae

were almost certainly in a periglacial state, with semi-permanent snow cover or permafrost conditions. Warming and melting that characterises the beginning of the Holocene would have resulted in a change in the stability of mountain slopes and rangefronts, thus enhancing the likelihood of very large rockmass failures such as LS1 and LS2. Therefore, we infer that landslides LS1 and LS2 were generated at the end of the LGM (transitioning into the Holocene). While we invoke a climatic argument for their formation, we acknowledge the strong possibility that the landslides could have been triggered by seismic shaking, such as would occur during rupture of the Clarence Fault or other proximal fault sources. Current paleoearthquake records do not extend to this time period, thus we can only suggest that very strong shaking was a triggering mechanisms for the emplacement of LS1 and LS2.

Are changes in the climate reflected in the sediment content of the lake? The fill in Lake McRae is characterised by low amplitude and high amplitude seismic facies. The older low amplitude and younger high amplitude acoustic facies have subequal thicknesses across the basin (Figure 5.6, Figure 5.7, Figure 5.8). We infer that the low amplitude facies are less organic-rich lake sediments that are characteristic of colder climate conditions when less vegetation was established around the lake. In contrast, the higher amplitude facies above them, are characteristic of higher organic content lake sediments (as seen from the shallow cores) that are indicative of warmer climate conditions. Thus, the transition from the Late Otiran or Late-Glacial to the Holocene may be broadly correlated with the change in acoustic facies within the lake. If this is the case then it is reasonable to assume that the early lake fill is pre-Holocene, and that the ^{10}Be cosmogenic age results are quite reasonable.

6.3 THE MOST RECENT FAULTING EVENT ON THE CLARENCE FAULT

In the lake section, slumped lake sediments and a turbidite can be observed interbedded within a suite of high amplitude (CHIRP) acoustic facies (Figure 5.7). The turbidite occurs within a small fault controlled basin adjacent to the trace of the Clarence Fault while the lake sediments have slumped into the main part of the lake basin. These are inferred to be co-eval shaking-derived mass wasting deposits that were caused by proximal fault rupture and shaking. We surmise that these deposits are related to the most recent faulting event on this central section of the Clarence Fault.

Using the shallow cores along with the radiocarbon dating model it is possible to bracket the timing of the turbidite. It is assigned a mean age of 1575 cal yr BP (range 1012-2166 cal yr BP). In Figure 5.7 we interpret the turbidite as filling the fault controlled basin and lapping onto the main strand of the Clarence Fault. At the scale that can be interpreted we infer that the turbidite overlies the most recent surface rupture of the fault, and is subsequently draped by undeformed hemipelagic lake sediments. No significant slumps or turbidites are observed in the lake section above these mass wasting units.

The trench excavated along the Clarence Fault reveals a series of colluvial deposits that could be interpreted as scarp- or rupture-derived colluvial wedges. We have erred against over-interpreting this record, as this is a shallow trench c.f. machine excavated trenches, so therefore some of the mapped units may be colluvial sub-units. In addition, we have not exposed any faults that can help demonstrate the relationships between individual colluviums.

Nonetheless, we observe a paleosol formed in colluvium that is overlain by quite young colluvium. The older colluvium formed at or before c. 1900-2000 cal yr BP. We infer that this colluvium is related to the most recent faulting event at Lake McRae.

Results from the lake indicate that the most recent faulting event on the central section of the Clarence Fault occurred 1000-2000 years ago. The timing of this event is as yet poorly constrained. The range is broadly coincident with the timing of the most recent faulting event on the eastern Clarence Fault which occurred 1700-1900 cal yr BP (Van Dissen and Nicol, 2009).

The lake record suggests there has been no surface faulting event in at least the last 1000 years, and possibly up to 1500-2000 years. We have estimated a dextral slip rate for the central Clarence Fault of 2.8 ± 1.4 mm/yr. Based on this rate the fault could accumulate between 1.4-8.4 m of slip (mean 4.2 m) over this time. These timing and slip data suggest that the central Clarence Fault is some way through its earthquake cycle.

6.4 Is Lake McRae a Useful Paleo-Seismometer?

A major goal of this project was to assess whether shaking-related deposits could be recognised within Lake McRae and whether these might be linked to historical and/or pre-historical seismic events. We have recognised and dated the most recent faulting event in the lake from CHIRP data and cores. We have also surmised that the very large LS1 and LS2 landslides could be seismically-triggered events. In addition, the rejuvenation of landslide LS2 by collapse into the lake (which arguably occurred at or above the boundary between low- and high-amplitude acoustic facies) could have also been seismically-triggered. Aside from the most recent turbidite and slumped lake sediments, the resolution of the CHIRP data is insufficient to be able to recognise any other mass wasting deposits within the upper, high-amplitude facies.

Does a signal of historical earthquake shaking exist within the lake record? For instance, was it possible to detect the shaking from the 1848, 1855, 1888 or 1929 earthquakes, or indeed has there been any evidence of shaking related disturbance form the 2016 Kaikoura earthquake? It has not been possible to come up with an equivocal answer to this. In the upper part of each of the cores it is recognised that there is a significant increase in sediment flux into the lake from the catchment. The sedimentation rate model derived from radiocarbon dates predicts that the peak of this change in rate occurred around 1866 AD (1723-1966 AD at 95%). The cause for this peak in increased sedimentation has been attributed to either: a) a change in the catchment due to pastoral farming practices of burning and grazing; or b) earthquake shaking. The former is favoured as the cause in this report. However, it is useful to note that only one historical event could be readily correlated with the change in sediment flux, i.e. the M 7.5 1848 Marlborough earthquake was of large enough magnitude and with low distance to produce MM intensity VIII shaking at Lake McRae. An initial reconnaissance of Lake McRae following the November 14, 2016 Kaikoura earthquake identified a slightly turbid lake in the days following the earthquake but little or no significant modification to the hillslopes surrounding the lake or related to the Goat Valley Stream catchment.

The results of this study indicate that Lake McRae has potential to yield data as a paleo-seismometer. The lake records proximal shaking and may record medial shaking from nearby sources such as the Awatere Fault. However, its location also means that it may not produce significant mass-wasting deposits or increased sediment flux from shaking that is weaker or from fault sources at a greater distance to the site. In that sense it acts as quite a sensitive indicator of regional earthquake shaking and could be used to assess the reliability of ground motion predictions for central and eastern Marlborough c.f. the National Seismic Hazard Model (Stirling et al., 2012).

7.0 CONCLUSIONS

A reconnaissance study of Lake McRae in central Marlborough has found that it has potential as a recorder of past shaking and fault-rupture events. Lake McRae formed near the end of the last glacial period when two very large landslides were emplaced across the east-west trending valley formed along the Clarence Fault. Landslides LS1 and LS2 could be seismically triggered. Landslide LS2 was rejuvenated in the early Holocene by a secondary failure at its northern front or toe. Sediments within the lake are consistent with latest Pleistocene and Holocene lake sedimentation within a filling lake in a warming environment, where the catchment became more (organically) productive. Analysis of geophysical data and shallow cores has provided evidence for the most recent proximal faulting event, which was the rupture of the central Clarence Fault 1000-2000 cal yr BP. This event was recognised by the presence of a turbidite and slumped lake sediments within the upper part of the lake section. Excavation into a fault scarp indicated that there is a colluvium that is consistent with the age of this event in the lake. A record of shaking related to the 1848 Marlborough earthquake (MM VIII) may exist within the top part of sediment cores, although this signal cannot be separated from an historical pastoral signal (grazing, burning) that could also have impacted the catchment of the lake.

This study has been of reconnaissance level only. There is potential for further significant research at Lake McRae. A list of potential future studies follows:

- Further cosmogenic dating of landslide deposits. Samples from an emergent boulder on LS2 could be collected and further samples could be collected from LS1
- The fault excavation trench could be extended (manually) to intercept faults. These faults could be of moderate dip and beyond the uphill extent of the current trench
- Latest Pleistocene to Holocene slip rates could be estimated from offset features. A suite of offset terraces has been recognised from LiDAR c. 1 km west of Lake McRae Hut. Paleoseismic data could be extracted from this site
- High resolution seismic data and long (6-m) sediment cores could be extracted from the lake
- Further reconnaissance as discussed above to test the effects of the 2016 Kaikoura earthquake.

8.0 ACKNOWLEDGMENTS

We wish to thank the Dept. of Conservation for allowing access to Lake McRae for research purposes and for use of the Lake McRae Hut. Jim Ward of Molesworth Station is thanked for accommodating of our field party at short notice and for access to the Molesworth airstrip. An NSF project awarded to Professor James Dolan provided LiDAR data that was used to help map and identify the geomorphology of the study area. Hanmer Helicopters provided great service to the lake at short notice. We thank Dr. Kevin Norton at Victoria University of Wellington for cosmogenic sample preparation and discussions about the systematics of the dating technique and Dr. Sebastien Huot (Illinois) for providing some IRSL dates at short notice. Finally, we thank Kate Clark and Mauri McSaveney for review comments that improved the readability of this report.

9.0 REFERENCES

Adams, J. 1981. Earthquake-dammed lakes in New Zealand. Geology 9:215-219.

Alloway, B.V.; Lowe, D.J.; Barrell, D.J.A.; Newnham, R.M.; Almond, P.C.; Augustinus, P.C.; Bertler, N.A.N.; Carter, L.; Litchfield, N.J.; McGlone, M.S.; Shulmeister, J.; Vandergoes, M.J.; Williams, P.W. 2007 Towards a climate event stratigraphy for New Zealand over the past 30,000 years (NZ-INTIMATE project). Journal of Quaternary Science, 22(1): 9-35.

Baisden, W.T., Prior, C.A., Chambers, D., Canessa, S., Phillips, A., Bertrand, C., Zondervan, A., Turnbull, J.C., Kaiser, J., and Bruhn, F., 2013. Rafter radiocarbon sample preparation and data flow: Accommodating enhanced throughput and precision: Nuclear Instruments & Methods in Physics Research, Section B, Beam Interactions with Materials and Atoms, v. 294, p. 194–198, doi: 10.1016 /j.nimb .2012 .07.014.

Balco, G., J.O. Stone, N.A. Lifton, and T.J. Dunai, 2008. A complete and easily accessible means of calculating surface exposure ages or erosion rates from 10Be and 26Al measurements, Quat. Geochron. 3: 174-195; http://hess.ess.washington.edu.

Barrell, D.J.A.; Andersen, B.G.; Denton, G.H. 2011 Glacial geomorphology of the central South Island, New Zealand. Lower Hutt: GNS Science. GNS Science monograph 27. 2 v

Bronk Ramsey, C., Lee, S. 2013. Recent and planned developments of the program OxCal: Radiocarbon, v. 55, p. 720–730, doi:10.2458/azu_js_rc.55.16215.

Browne, G.H. 1992. The northeastern portion of the Clarence Fault: tectonic implications for the late Neogene evolution of Marlborough, New Zealand. New Zealand Journal of Geology and Geophysics, 35(4): 437-445.

Chapron, E.; Beck, C.; Pourchet, M.; Deconinck, J. F. 1999. 1822 earthquake-triggered homogenite in Lake Le Bourget (NW Alps). Terra Nova, v. 11, no. 2-3, p. 86-92.

Cowan, H. A. 1991. The North Canterbury earthquake of September 1, 1888. Journal of the Royal Society of New Zealand 21, 1-12.

Cruden D.M., Varnes D.J., 1996. Landslide types and processes. In: Turner AK, Schuster RL (eds) Landslides: investigation and mitigation (Special Report). Washington, DC, USA: National Research Council, Transportation and Research Board Special Report 247, pp 36–75.

Ditchburn, R., A. Zondervan, S. Mawdesley, and J. Futter (2014), An improved method for separating quartz from rock using pyrophosphoric acid, GNS Science Report 2014/45.

Debret, M., Sebag, D., Desmet, M., Balsam, W., Copard, Y., Mourier, B., Susperrigui, A. S., Arnaud, F., Bentaleb, I., Chapron, E., Lallier-Vergès, E., and Winiarski, T., 2011. Spectrocolorimetric interpretation of sedimentary dynamics: The new “Q7/4 diagram”: Earth-Science Reviews, v. 109, no. 1–2, p. 1-19.

DeMets, C., Gordon R.G., Argus, D.F., 2010. Geologically current plate motions. Geophysical Journal International 181: 1-80.

DeMets, C.; Gordon, R.G.; Argus, D.F.; Stein, S. 1994. Effect of recent revisions to the geomagnetic reversal time scale on estimates of current plate motions. Geophysical Research Letters 21: 2191-2194.

Downes, G.L.; Dowrick, D.J. 2014. Atlas of isoseismal maps of New Zealand earthquakes - 1843-2003 2nd edition (revised). GNS Science Monograph 25. CD

Dunai, T.J. 2010. Cosmogenic nuclides: principles, concepts and applications in the earth surface sciences, Cambridge University Press, ISBN 978-0-521-87380-2.

Eusden, J.D.; Upton, P.; Eichelberger, N.; Pettinga, J.R. 2012. The Dillon and Acheron sinistral faults, Marlborough Fault System, New Zealand: field studies and mechanical modelling. New Zealand Journal of Geology and Geophysics. 55(2): 91-102.

Goehring, B.M.; Muzikar, P.; N.A. Lifton 2013. An in situ 14C-10Be Bayesian isochron approach for interpreting complex glacial histories, Quat. Geochron. 15: 61-66.

Gosse, J.C.; Phillips, F.M. 2001.Terrestrial in situ cosmogenic nuclides: theory and application. Quat. Sci. Rev. 20: 1475-1560.

Grapes, R.; Little, T.; Downes, G. 1998. Rupturing of the Awatere Fault during the 1848 October 16 Marlborough earthquake, New Zealand: historical and present day evidence. New Zealand Journal of Geology and Geophysics 41: 387-400.

Hamling, I.J.; D'Anastasio, E.; Wallace, L.M.; Ellis, S.M.; Motagh, M.; Samsonov, S.; Palmer, N.G.; Hreinsdottir, S. 2014 Crustal deformation and stress transfer during a propagating earthquake sequence: the 2013 Cook Strait sequence, Central New Zealand. Journal of Geophysical Research. Solid Earth, 119(7): 6080-6092; doi: 10.1002/2014JB011084.

Hancox, G.T.; Perrin, N.D. 2009 Green Lake landslide and other giant and very large postglacial landslides in Fiordland, New Zealand. Quaternary Science Reviews 28:1020–1036.

Hancox, G.T.; Carey, J.M. 2013. Assessment of rock fall risk at Mintaro Hut site on the Milford Track, and evaluation of potential new sites for Mintaro Hut in the upper Clinton valley, Fiordland National Park. GNS Science consultancy report 2012/315. 30 p.

Hancox, G.T.; Dellow, G.; Perrin, N.D. 2002. Recent studies of historical earthquake-induced landsliding, ground damage, and MM intensity in New Zealand. Bulletin of the New Zealand Society for Earthquake Engineering, 35(2): 59-95.

Hancox, G.T., Langridge, R.M.; Perrin, N.D.; Vandergoes, M.; Archibald, G. 2013. Recent mapping and radiocarbon dating of three giant landslides inn northern Fiordland, New Zealand. GNS Science Report 2012/45, 52 p.

Hancox, G.T.; Archibald, G.C.; Cousins, W.J., Perrin, N.D., Misra, S. 2014. Recent Reconnaissance report on liquefaction effects and landslides caused by the ML 6.5 Cook Strait earthquake of 21 July 2013, New Zealand. GNS Science Report 2013/42, 20 p.

Hogg, A.G.; Hua, Q.; Blackwell, P.G.; Niu, M.; Buck, C.E.; Guilderson, T.P.; Heaton, T.J.; Palmer, J.G.; Reimer, P.J.; Reimer, R. W.; Turney, C.S.M.; Zimmerman, S.R.H. 2013. SHCal13 Southern Hemisphere Calibration, 0-50,000 Years cal BP. Radiocarbon 55: 1889–1903.

Howarth, J. D.; Fitzsimons, S.J.; Jacobsen, G.E.; Vandergoes; M.J.; Norris, R.J. 2013. Identifying a reliable target fraction for radiocarbon dating sedimentary records from lakes: Quaternary Geochronology, 17: 68-80, doi.org/10.1016/j.quageo.2013.02.001.

Howarth, J.D.; Fitzsimons, S.; Norris, R.J. 2012. Lake sediments record cycles of sediment flux driven by large earthquakes on the Alpine fault, New Zealand. Geology 40(12): 1091-1094.

Howarth, J.D.; Fitzsimons, S.J.; Norris, R.J.; Jacobsen, G.E. 2014. Lake sediments record high intensity shaking that provides insight into the location and rupture length of large earthquakes on the Alpine Fault, New Zealand. Earth and Planetary Science Letters, 403: 340-351; doi: 10.1016/j.epsl.2014.07.008.

Howarth, J.D., Fitzsimons, S.J.; Norris, R.J.; Langridge, R.; Vandergoes, M.J. 2016. A 2000 yr rupture history for the Alpine fault derived from Lake Ellery, South Island, New Zealand. Geological Society of America Bulletin v. 128, p. 627-643, doi:10.1130/B31300.1.

Hua, O.; Jacobsen, G.E.; Zoppi, U.; Lawson, E.M.; Williams, A.A.; McGann, M.J. 2001. Progress in radiocarbon target preparation at ANTARES AMS Centre: Radiocarbon, v. 432A, p. 275–282.

Kaiser, A.; Holden, C.; Beavan, J.; Beetham, D.; Benites, R.; Celentano, A. Collett, D.; Cubrinowski, M.; Denys, P.; Fielding, E.; Fry, B.; Gerstenberger, M.; Langridge, R.; Massey, C.; Motagh, M.; Pondard, N.; McVerry, G.; Ristau, J.; Stirling, M.; Thomas, J.; Uma, S.R.; Zhao, J. 2012. The Mw 6.2 Christchurch earthquake of February 2011: Preliminary Report. New Zealand Journal of Geology and Geophysics 55: 67-90. doi: 10.1080/00288306.2011.641182.

Khajavi, N.; Quigley, M.; McColl, S.T.; Rezanejad, A. 2012. Seismically induced boulder displacements in the Port Hills, New Zealand during the 2010 Darfield (Canterbury) earthquake. New Zealand Journal of Geology and Geophysics 55: 271-278.

Khajavi, N.; Langridge R.M.; Quigley, M.C.; Smart, C.; Rezanejad, A.; Martin-Gonzalez, F. 2016. Late Holocene rupture overlap and earthquake clustering on the Hope Fault, New Zealand. Geological Society of America Bulletin 128: doi:10.1130/B31199.1

Kieckhefer, R.M. 1979: Sheets M31D, N31A, N31C, and parts of M32A and M32B Leader Dale (1st edition), Sheets N31B and N31D Dillon (1st Edition) "Late Quaternary Tectonic Map of New Zealand 1:50 000". 3 maps and text (28 p.) Department of Scientific and Industrial Research, Wellington, New Zealand

Kohl, C.P.; Nishiizumi, K. 1992.Chemical isolation of quartz for measurement of in-situ-produced cosmogenic nuclides, Geochim. Cosmochim. Acta 56: 3583-3587.

Langridge, R.M. 2004. How is tectonic slip partitioned from the Alpine Fault to the Marlborough Fault System? – Results from a FRST Post-Doctoral Fellowship, Institute of Geological & Nuclear Sciences science report 2004/32. 18 p.

Langridge, R.M.; Berryman, K.R. 2005. Morphology and slip rates of the Hurunui section of the Hope Fault, South Island, New Zealand. New Zealand Journal of Geology and Geophysics, 48(1): 43-57

Langridge, R.M.; Campbell, J.; Hill, N.L.; Pere, V.; Pope, J.; Pettinga, J.; Estrada, B.; Berryman, K.R. 2003. Paleoseismology and slip rate of the Conway Segment of the Hope Fault at Greenburn Stream, South Island, New Zealand. Annals of Geophysics, 46(5): 1119-1139.

Langridge, R.; Van Dissen, R.; Rhoades, D.; Villamor, P.; Little, T.; Litchfield, N.; Clark, K.; Clark, D. 2011. Five thousand years of surface ruptures on the Wellington Fault, New Zealand: Implications for recurrence and fault segmentation. Bulletin of the Seismological Society of America 101 (5): 2088-2107.

Langridge, R.M.; Almond, P.C.; Duncan, R.P. 2013. Timing of late Holocene paleoearthquakes on the Hurunui segment of the Hope fault: Implications for plate boundary strain release through South Island, New Zealand. Geological Society of America Bulletin, doi:10.1130/B30674.1.

Little, T.A.; Jones, A. 1998. Seven million years of strike-slip and off-fault deformation on the Awatere Fault, South Island, New Zealand. Tectonics 17: 285-302.

MacKereth, F.J.H. 1958. A portable core sampler for lake deposits: Limnology and Oceanography, v. 3, p. 181–191, doi:10.4319/lo.1958.3.2.0181.

Massey, C.I.; McSaveney, M.J.; Lukovic, B.; Heron, D.W.; Ries, W.; Moore, A.; Carey, J.M. 2012. Canterbury earthquakes 2010/11 Port Hills slope stability: life-safety risk from rockfalls (boulder rolls) in the Port Hills. GNS Science consultancy report 2012/123. 29 p.

Newsome, P.F.J. 1987. The vegetative cover of New Zealand. National Water and Soil Conservation Authority. Water and Soil Miscellaneous Publication 112, 153 p. + 2 map sheets.

Nicol, A.; Van Dissen, R.J. 2002: Up-dip partitioning of displacement components on the oblique-slip Clarence Fault, New Zealand. Journal of Structural Geology 24:1521-1535.

Nishiizumi, K.; Imamura, M.; Caffee, M.W.; Southon, J.R.; Finkel, R.C.; McAninch, J. 2007. Absolute calibration of 10Be AMS standards, Nucl. Instrum. Meth. B 258: 403-413.

Rattenbury, M.S.; Townsend, D.B.; Johnston, M.R. (compilers) 2006. Geology of the Kaikoura area. Institute of Geological & Nuclear Sciences 1:250,000 geological map 13. 1 sheet + 70 p. Lower Hutt, New Zealand: GNS Science.

Reyners, M.; McGinty, P.; Gledhill, K.; O'Neill, T.; Matheson, D.; Cousins, J.; Zhao, J.; McVerry, G.; Cowan, H.; Hancox, G.; Cox, S.; Turnbull, I.; Caldwell, G.; and the GeoNet team. 2003. The Mw 7.2 Fiordland earthquake of August 21, 2003: background and preliminary results. Bulletin of the New Zealand Society for Earthquake Engineering, Bull. N.Z Nat. Soc. Vol. 36: number 4

Sebag, D.; Debret, M.; M'Voubou, M.; Obame, R. M.; Ngomanda, A.; Oslisly, R.; Bentaleb, I.; Disnar, J.R.; Giresse, P. 2013. Coupled Rock-Eval pyrolysis and spectrophotometry for lacustrine sedimentary dynamics: Application for West Central African rainforests (Kamalete and Nguene lakes, Gabon): Holocene 23, no. 8, p. 1173-1183.

Schnellmann, M.; Anselmetti, F. S.; Giardini, D.; McKenzie, J. A.; Ward, S.N. 2002. Prehistoric earthquake history revealed by lacustrine slump deposits. Geology 30: 1131-1134.

Schnellmann, M.; Anselmetti, F. S.; Giardini, D.; McKenzie, J. A. 2006. 15,000 years of mass-movement history in Lake Lucerne: Implications for seismic and tsunami hazards: Eclogae Geologicae Helvetiae, v. 99, no. 3, p. 409-428.

Stirling, M.W.; Anooshehpoor, R. 2006. Constraints on probabilistic seismic-hazard models from unstable landform features in New Zealand. Bulletin of the Seismological Society of America, 96(2): 404-414.

Stirling, M.W.; McVerry, G.H.; Berryman, K.R. 2002. A new seismic hazard model for New Zealand. Bulletin of the Seismological Society of America, 92(5): 1878-1903.

Stirling, M.W.; McVerry, G.; Gerstenberger, M.; Litchfield, N.; Van Dissen, R.; Berryman, K.; Barnes, P.; Wallace, L.; Villamor, P.; Langridge, R.; Lamarche, G.; Nodder, S.; Reyners, M., Bradley, B.; Rhoades, D., Smith, W., Nicol, A., Pettinga, J., Clark, K. and Jacobs., K. 2012. National Seismic Hazard Model for New Zealand: 2010 Update. Bulletin of the Seismological Society of America 102 (4): 1514-1542, doi: 10.1785/0120110170.

Strasser, M.; Monecke, K.; Schnellmann, M.; Anselmetti, F. S. 2013. Lake sediments as natural seismographs: A compiled record of Late Quaternary earthquakes in Central Switzerland and its implication for Alpine deformation: Sedimentology 60: 319-341.

Townsend, D.B.; Little, T.A. 1998. Pliocene-Quaternary deformation and mechanisms of near-surface strain close to the eastern tip of the Clarence Fault, northeast Marlborough, New Zealand. New Zealand Journal of Geology and Geophysics 41: 401-418.

Van Dissen, R. 1989: Late Quaternary faulting in the Kaikoura region, southeastern Marlborough, New Zealand. Unpublished MS thesis, Oregon State University, USA: 72 p.

Van Dissen, R.; Nicol, A. 2009. Mid-late Holocene paleoseismicity of the eastern Clarence Fault, Marlborough, New Zealand. New Zealand Journal of Geology and Geophysics 52(3): 195-208.

Van Dissen, R.; Yeats, R.S. 1991. Hope fault, Jordan thrust, and uplift of the Seaward Kaikoura Range, New Zealand. Geology 19: 393-396.

Wright, C.A. 1998. The AD 930 long-runout Round Top debris avalanche, Westland, New Zealand. New Zealand Journal of Geology and Geophysics 41(4): 493-497.

Zondervan, A.; Hauser, T.M.; Kaiser, J.; Kitchen, R.L.; Turnbull, J.C.; West, J.G. 2015. XCAMS: The compact 14C accelerator mass spectrometer extended for 10Be and 26Al at GNS Science, New Zealand, Nucl. Instrum. Meth. B 361: 25-33.

APPENDICES

This page is intentionally left blank.

A1.0 APPENDIX 1

Summary of field trip activities:

Two initial field plans were hampered by bad weather in April (Cyclone Ita) and November 2014 that postponed the field reconnaissance until March 2015. The tail end of Cyclone Pam also disrupted our field plans resulting in a change of helicopter operator in order to get the scientific team and payload into Lake McRae. This resulted in a loss of 1 day of field time. We used Hanmer Helicopters and were picked up and dropped at the Molesworth airfield, Marlborough.

The field reconnaissance proceeded as follows:

Thursday March 19th

- Early morning flight into lake; gear drop at lake and hut
- Assembly of inflatable boats
- Collection of geophysical data from the lake
- Reconnaissance of LS1 landslide, Clarence Fault trace, and LS2 landslide
- Assessment of greywacke tors and boulders on LS1 for Cosmogenic dating.

Access around the lake was enabled by inflatable boat.

Friday March 20th

- Excavation and logging of trench along Clarence Fault
- Completion of geophysical data acquisition from the lake
- Preliminary lake sediment coring
- Initial sampling of greywacke tors and boulders on LS1.

Saturday March 21st

- Trench sampling and infill
- Completion of lake sediment coring
- Further sampling of greywacke tors and boulders on LS1
- Pack up of gear and helicopter pick-up.